공학석사 학위논문

Study on a Procedure of Structural Safety Assessment for an Energy Saving Device Subjected to Hydrodynamic Force

유체력을 받는 에너지절감장치의 구조안전성 평가절차에 관한 연구

2015 년 02 월

서울대학교 대학원

조선해양공학과

이 동 범

Study on a Procedure of Structural Safety Assessment for an Energy Saving Device Subjected to Hydrodynamic Force

지도 교수 장 범 선

이 논문을 공학석사 학위논문으로 제출함

2015 년 2 월

서울대학교 대학원

조선해양공학과

이 동 범

이동범의 공학석사 학위논문을 인준함

2015 년 2 월

위 원 장 양 영 순 (인)

부위원장 조 선 호 (인)

위 원 이 신 형 (인)

Abstract

Study on a Procedure of Structural Safety Assessment for an Energy Saving Device Subjected to Hydrodynamic Force

Lee DongBeom

Department of Naval Architecture and Ocean Engineering

The Graduate School

Seoul National University

Due to the soaring oil price and the demand of CO_2 reduction related to environmental issues, the demand for the reduction of fuel oil consumption is greater than ever before. In this respect, various types of energy saving devices (ESD) have been developed. ESD is

a kind of fin placed along streamline and installed around propeller or stern to improve the propulsive performance. The main direction of hydrodynamic force on the fin is nearly same as the streamline, and its magnitude may be negligible in calm sea. However, in harsh environment, the heave and pitch motion of a vessel becomes larger and the fin-shaped ESD would experience large out-of-plane load and there is a high risk of structural failure and fatigue damage. In a conventional design approach, Morison's equation may be adopted with constant coefficient for hydrodynamic force evaluation. Spectral approach has been also widely used based on the assumption of linear system. However, it is difficult for Morison's equation and spectral method to estimate hydrodynamic force exactly.

Therefore, this study proposes a new procedure of structural safety assessment for energy saving devices (ESD) subject to hydrodynamic force and applies the proposed procedure to the fin-type energy saving device.

The proposed safety assessment procedure consists of three main parts, seakeeping analysis, computational fluid dynamics (CFD) analysis and long-term analysis. As the sea-keeping analysis, potential based commercial code, WASIM, is used. Response amplitude operators (RAO) and response spectrums of vertical velocity at ESD are calculated. In CFD analysis, Hydrodynamic force are calculated for predefined regular waves using VOF (Volume of Fluid) and DFBI (Dynamic Fluid Body Interaction) techniques and a neural network is trained using the data. Irregular time histories of vertical velocities are generated from response spectrums obtained from sea-keeping analysis. In order to take into account the randomness of the irregularity, twenty different irregular time histories are generated. Then, each time history of vertical velocity is converted to time histories of hydrodynamic force. For each sea state, twenty maximum hydrodynamic force values for 3 hours duration are collected and Gumbel distribution is used to fit the data. This process is repeated for all sea states in wave scatter diagram and long-term value is calculated. An approximate long-term calculation is made using contribution coefficient based method. The method enables to carry out time domain analysis for a part of sea states that have dominant contributions to long-term exceedance probability. The contribution coefficients of all sea states can be calculated from frequency domain with less computational time. As a result, the total computation time for long-term analysis is reduced.

Additionally, a procedure of fatigue strength assessment is established. 3 hours' time series of vertical velocity is generated from the response spectrum and the peak values of vertical velocity are transferred to lift force and moment using the trained neural network. The time series of lift force and moment are transferred to stress histogram using a stress response per unit force. Finally, fatigue damage is calculated using Miner's rule.

Keywords : ESD(Energy Saveing Device), CFD(Computational Fluid Dynamics), Neural network, Long-term analysis

Student Number : 2013-21074

Contents

List of Figures

List of Tables

1. Introduction

1.1. Research background and status

Due to the soaring oil price and the demand of CO_2 reduction related to environmental issues, the demand for the reduction of fuel oil consumption is greater than ever before. In this respect, various types of energy saving devices (ESD) have been developed as shown in Fig. 1. They are installed around propeller or stern to improve the propulsive performance. ESD is a kind of fin placed along stream line. The main direction of hydrodynamic force on the fin, drag force, is nearly same as the stream line and its magnitude may be negligible in calm sea.

However, in harsh environment, the heave and pitch motion of a vessel becomes larger and the fin-shaped ESD would experience large out-of-plane load, lifting force, and there is a high risk of structural failure and fatigue crack. In actual, such cracks have been reported in some vessels.

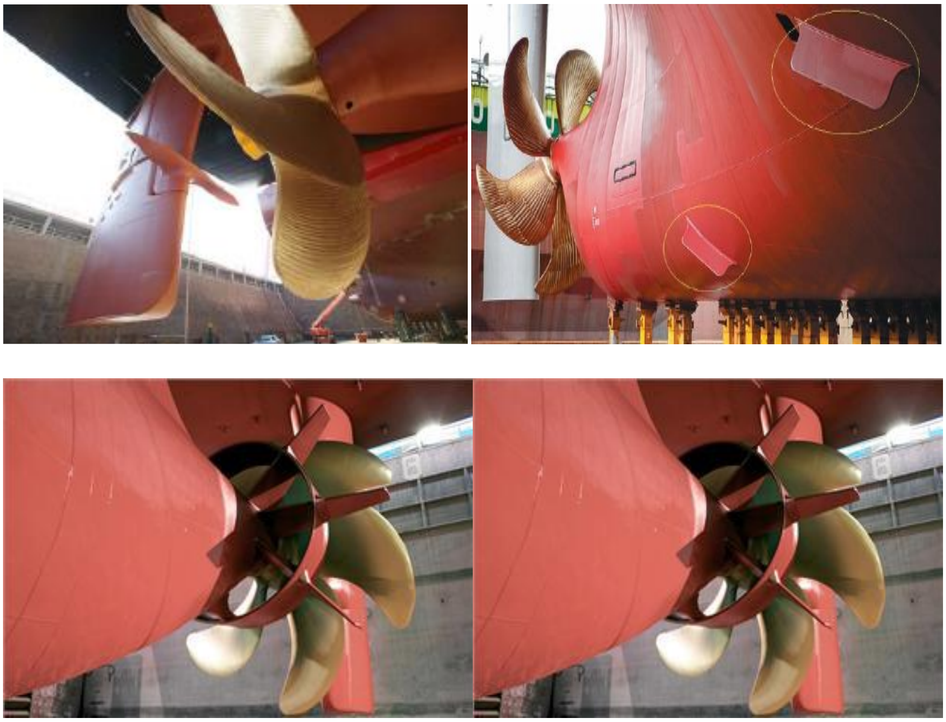

Fig 1 Various types of energy saving devices

For a steady flow passing a thin streamlined section at a small angle of attack, smooth tangential steam lines form on the hydrofoil. Then, viscous effect is confined to thin boundary layer on the foil surface. In the case of a symmetric foil, lift force is known to be proportional to the angle of attack when the angle is small. As the angle of attack grows, the lift coefficient reaches its maximum at certain angle. If the angle of attack goes beyond this critical angle, fluid starts to separate from a hydrofoil. Then, the force is regarded as Morison's force. In a conventional design approach, Morison's equation may be adopted with constant coefficient for hydrodynamic force evaluation. It assumes that total hydrodynamic force is a sum of inertial force and viscous force.

Meanwhile, for a conventional strength assessment and fatigue analysis in linear system, spectral approach has been widely used based for an assessment of strength and fatigue. Woo et al [1] presented strength and fatigue assessment of duct type energy saving device based on the assumption of linear transfer function as shown in Fig. 2. However, the nonlinearity of the viscous force is a major obstacle in the use of conventional spectral method.

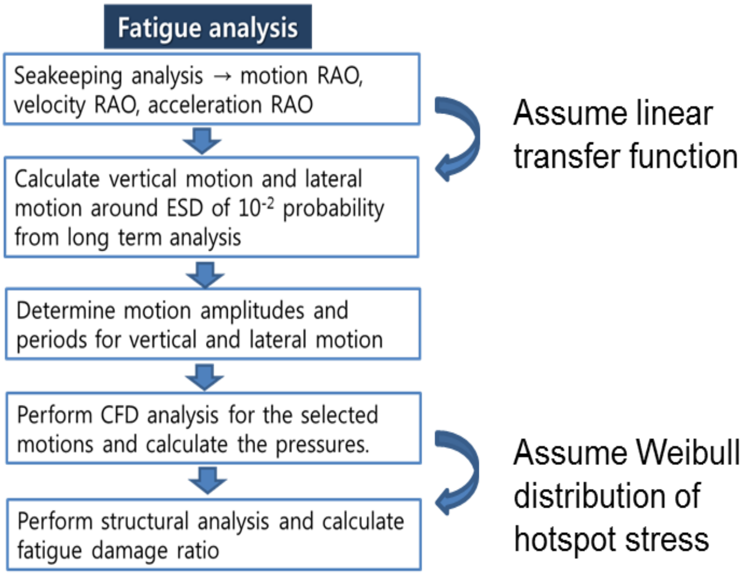

Fig 2 Simplified fatigue assessment based on linear transfer function

1.2. Research objective

This study aims at predicting hydrodynamic loads on ESD using CFD analysis and applying it to the structural model for estimation of structural safety.

As a first step to establish the procedure of structural safety assessment for ESD, this research focused on the characteristic of hydrodynamic force such as nonlinearity of drag force, relation among inlet flow velocity, vertical velocity, lift and drag force using computational fluid dynamics (CFD). It is described in Section 2.

Then, hydrodynamic load estimation using CFD analysis and long-term analysis for lift force and moment are performed. Finally, ultimate and fatigue strength are evaluated using the calculated load. The contents are unfolded as follows. Section 3 describes ship motion analysis using potential-based commercial code, DNV.WASIM, and CFD analysis. The validity of CFD analysis is proved through a comparison with WASIM results. In Section 4, hydrodynamic forces such as shear force and bending moment imposed on ESD are calculated using CFD analysis for full ship model. Long-term analysis for the hydrodynamic forces is carried out in Section 5 and global strength assessment is performed in Section 6. Finally, fatigue strength assessment is performed in Section 7.

2. Investigation of characteristic of hydrodynamic force using three different models

2.1. Model description

In order to obtain hydrodynamic force by the fluid on the hydrofoil, numerical simulations using the hydrofoil describing the motions specified are implemented. Fluent, a commercial CFD software, is used for all the calculations. Also, dynamic mesh function, bring the benefits of easier setup to simulate the vertical motion of the hydrofoil, is used.

The NACA0012, as well known cross-sectional geometry, is used for the analysis and the geometrical property is shown in Fig.3 [2]. The cross section is symmetrical and has no camber. The chord length is 1.0 m, and the thickness is 12% of the chord length. The angle of attack is assumed 0 degree.

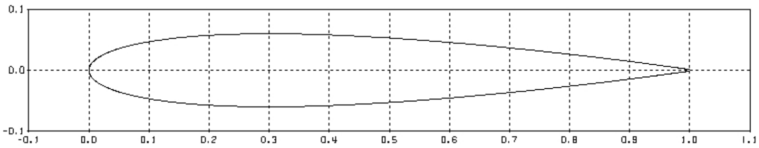

Fig 3 Geometry of NACA0012

The realizable k−ε model is used to solve RANS equation. Boundary condition for the hydrofoil is set as no−slip wall with standard wall function. To capture the fluid dynamics around the hydrofoil, y+ ranges between 40 and 150. Moving zone located at the mid of the domain plunges by a user defined function, whereas the upper and lower domains are fixed. The details of simulation setting are listed in Table 1.

Table 1 Numerical method

Software	Fluent 14.5.7
Turbulence model	Realizable k−ε
Scheme	PISO
Turbulent Kinetic Energy	Third−order MUSCL
Turbulent Dissipation Rate	Third−order MUSCL
Time step size(s)	0.001
Iteration/time step	100

In this study, inlet flow velocity increases from 8.0m/s to 20.0 m/s in 6.0 m/s steps. The hydrofoil oscillates vertically, that is, perpendicularly to the inlet flow, and the vertical motion is defined as follows: The amplitude (A) of the motion is 1.0 m. Vertical velocity is expressed as $U(t) = A\omega \sin(\omega t)$ and the maximum velocity ranges from 6.28m/s to 11.0 m/s by varying angular frequency(ω) from 2π to 3.5π. Fig. 4 shows the example of the oscillating motion. The oscillating frequency is fixed at 1.75 Hz and the vertical velocity reaches its maximum of vertical velocity at 11.0 m/s when the foil passes the mid−level in the oscillation and zero at the highest and the lowest levels. Due to the vertical oscillation, the attack angle of inlet flow changes continuously.

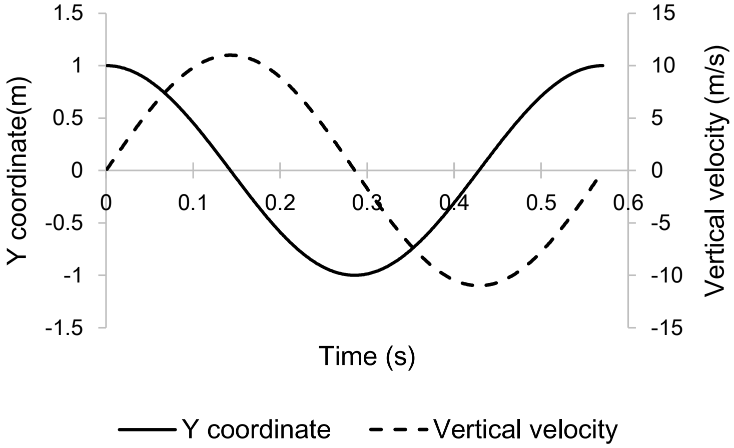

Fig 4 Motion of hydrofoil

Two dimensionless parameters, lift coefficient and drag coefficient, are investigated in this study. The parameters are expressed as below.

$$C_L = \frac{F_L}{\frac{1}{2}\rho S U^2} \quad \text{and} \quad C_D = \frac{F_D}{\frac{1}{2}\rho S U^2}$$

Where, F_L=lift force, F_D=drag force, ρ=density of fluid, S= plane area of the hydrofoil, U = Inlet velocity of foil

To investigate characteristics of hydrodynamic force on the hydrofoil, three kinds of models that represent two-dimensional domain, simplified three-dimensional domain and detailed three dimensional domain approach respectively are simulated as below.

Model I : 2D simulation

In this model, the hydrofoil (1.0 m in length and 0.12 m in depth) is placed at the middle of the computation domain defined as 40.0 m in length and 40.0 m in depth. Velocity Inlet and pressure outlet boundary conditions are applied on the left and right sides of the domain. In addition, wall condition is applied on the top and bottom of the computational domain. Fig.5 shows CFD model with the oscillating motion of hydrofoil in computational domain.

Model II : 3D simulation with one-sided wall

In this simulation, the hydrofoil (1.0m in length, 0.12m in depth and 3.2 m in span) is placed at 10.0 m behind the inlet face of the computational domain defined by a length of 30.0 m, a depth of 40.0 m and a width of 32.0 m. For the computational domain, velocity inlet and pressure outlet boundary conditions are applied on the front and back faces, and a wall condition is applied on the bottom, top, right and left faces. The detail is depicted in Fig.6.

Model III : 3D simulation with hull form

In this simulation, the hydrofoil (1.0 m in length, 0.12m in depth and 3.2 m in span) is placed at the forward part of the computation domain which is defined by a length of 445.0 m, a depth of 79.5 m and a width of 75.0 m. For the simulation including hull form, the forward part at the midship is eliminated to save computational time based on the assumption that it will not affect to the fluid flow at the aft body importantly. On the computational domain, Velocity inlet and pressure outlet boundary conditions are applied on the front and back faces, and a symmetric condition is applied on the right and the top face to reduce the number of element and consider free-surface effect. Inlet boundary condition is also imposed on the left face. The detail is shown in Fig.7 and 8.

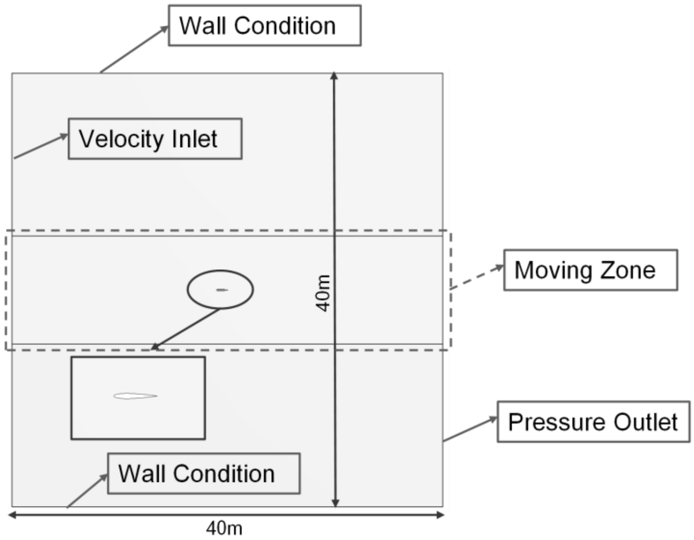

Fig 5 Detail of 2D simulation (Model I)

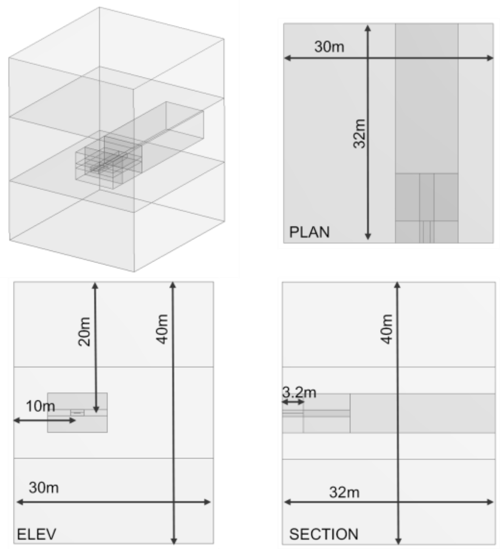

Fig 6 Detail of 3D simulation with one-sided wall (Model II)

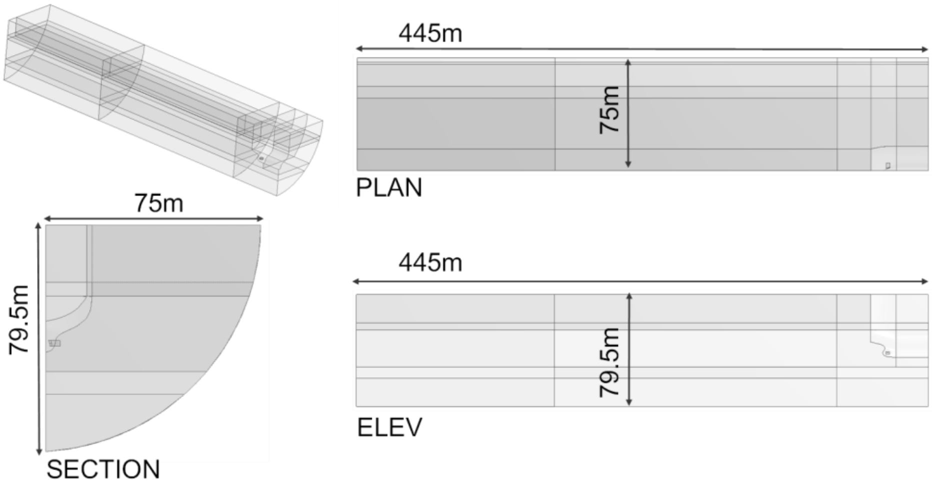

Fig 7 Detail of 3D simulation with hull form (Model III)

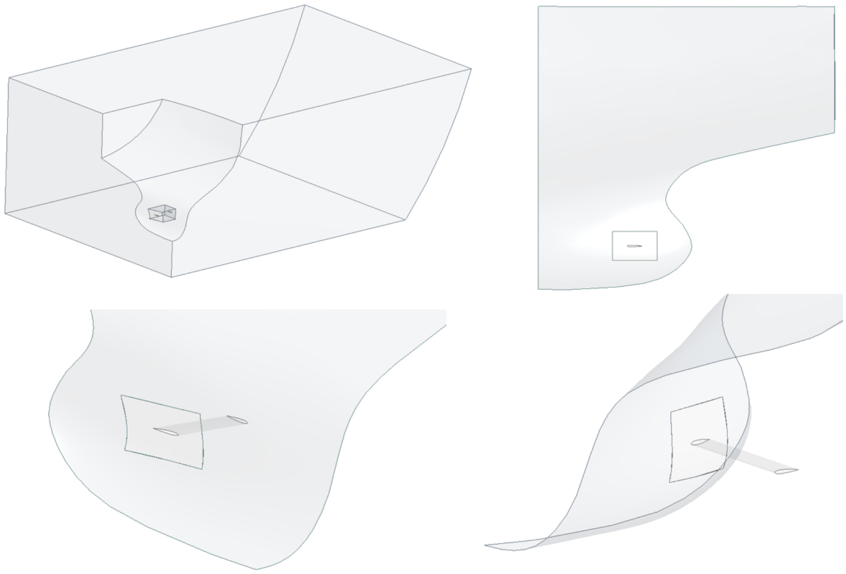

Fig 8 Detail of hydrofoil (Model III)

2.2. Relation between inlet flow velocity and lift and drag coefficient

In this section, the relation between inlet flow velocity and hydrodynamic force will be investigated and discussed. Fig.9 shows relations between inlet flow velocity and hydrodynamic force. The result indicates that drag and lift forces increase as the inlet flow becomes faster and the lift force reaches its maximum at the peak of vertical velocity time history while the peaks of the drag force don’t match with those of vertical velocity. The proportion of drag force to lift force is about 10% because the foil has large projected are in the vertical direction, and the magnitude of the vertical velocity is not much different with the inlet velocity.

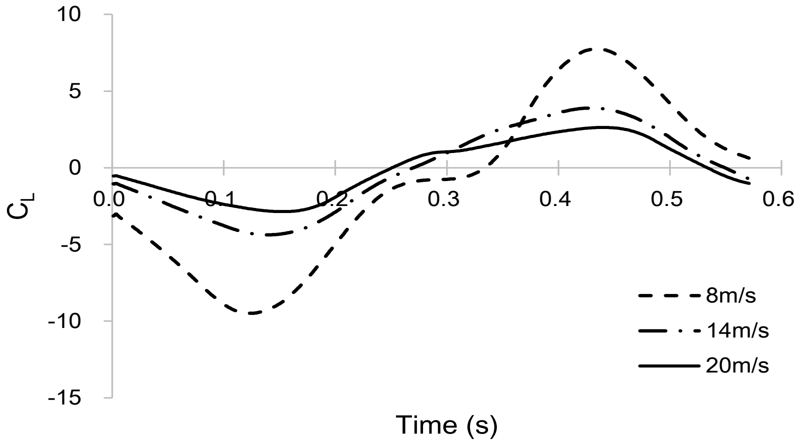

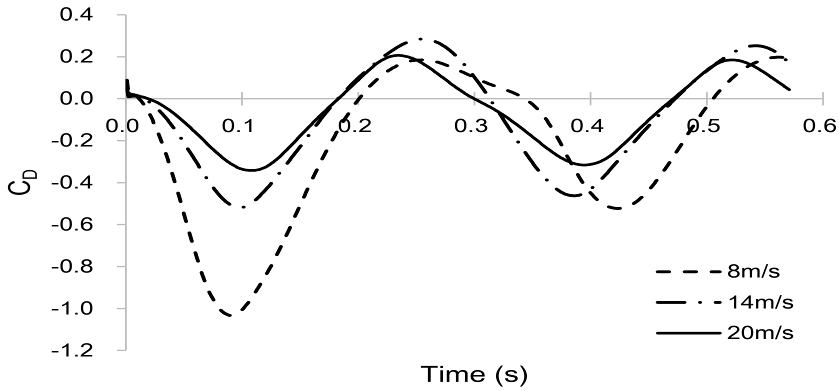

Fig 9 Inlet flow velocity vs lift and drag coefficient (Model I)

Fig.10 and Fig. 11 show the correlation between inlet flow velocity and lift force. Lift coefficient is gradually reduced as inlet flow velocity increases. However, lift force becomes larger because the lift force is calculated by multiplying the lift coefficient to the square of inlet flow velocity. As can be seen from Fig.11, nonlinearity of lift force increases as vertical velocity increases. Therefore, it is necessary to make a proper approach to reasonably treat the nonlinearity of the lifting force calculated from CFD.

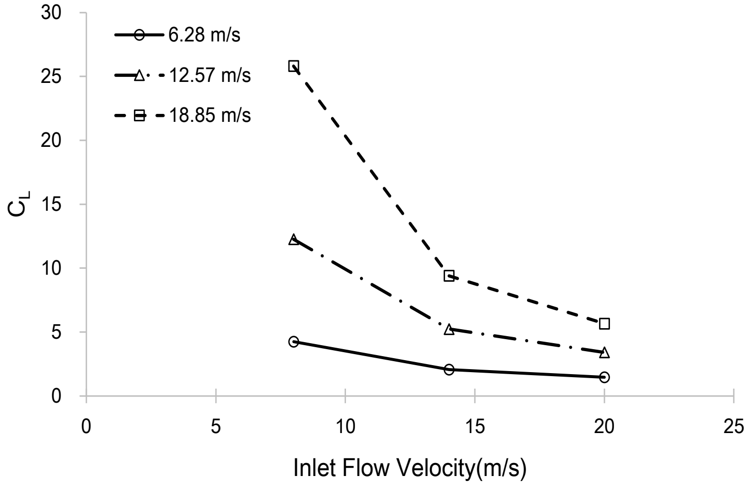

Fig 10 Inlet flow velocity vs C_L (Model I)

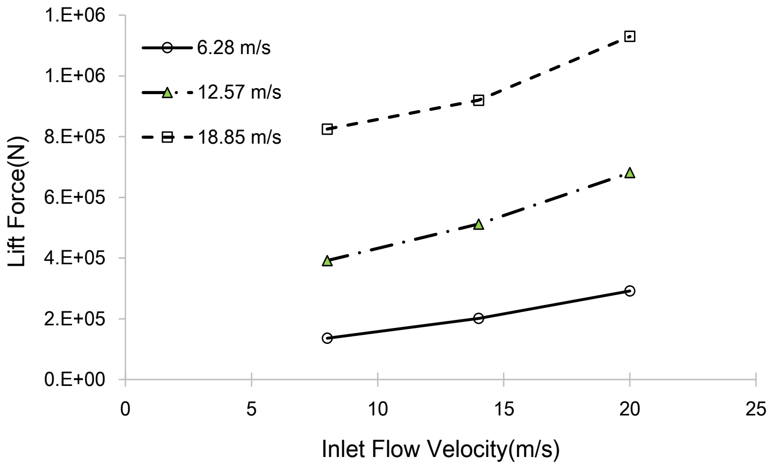

Fig 11 Inlet flow velocity vs lift force (Model I)

2.3. Relation between vertical velocity and hydrodynamic force

Lift and drag forces for different vertical velocities with a uniform inlet flow velocity are presented in Fig.12. The inlet velocity is fixed at 20.0 m/s, and the oscillating frequency ranges from 1.0 Hz to 1.75 Hz. Fig.14 shows that as vertical velocity becomes higher, lift force also increase. Lift force becomes maximum value at the max vertical velocity while the moment of the maximum value of drag force does not coincide with that of max vertical velocity.

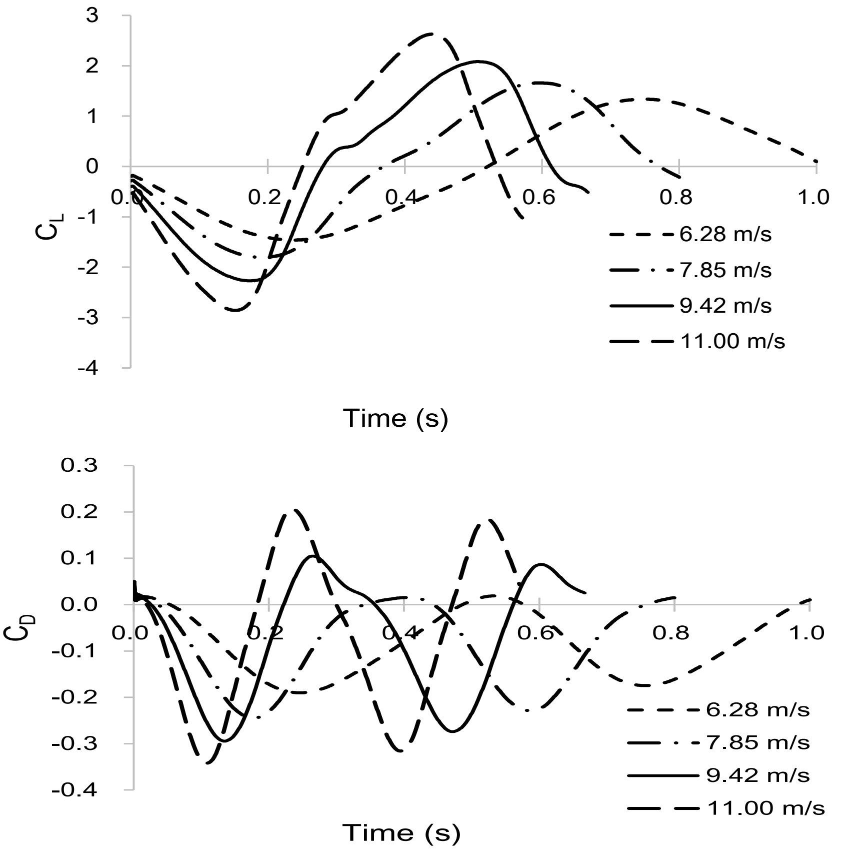

Fig 12 Vertical velocity vs drag coefficient (Model I)

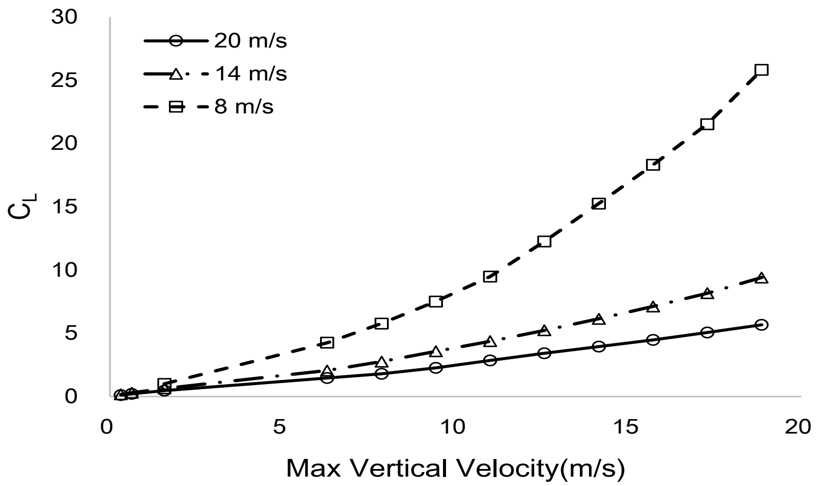

Fig 13 Max vertical velocity vs C_L (Model I)

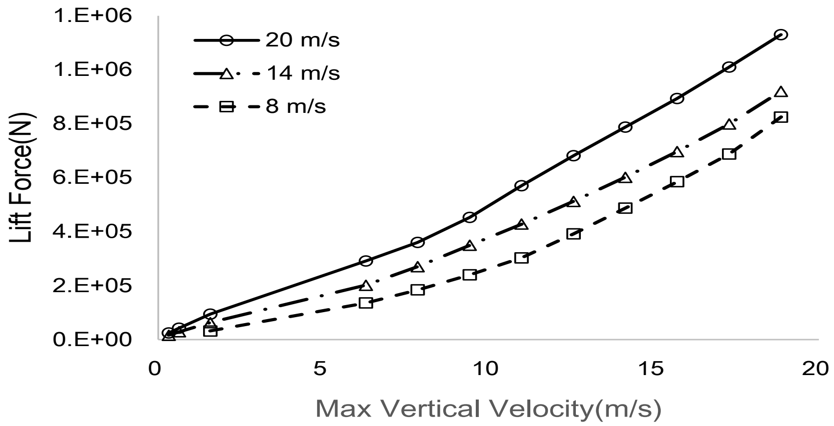

Fig 14 Max vertical velocity vs lift force (Model I)

Fig.13 and Fig. 14 indicate the correlation between maximum vertical velocity and lift force. Similarly, to the relation between the inlet flow velocity and lift force, the lift force becomes larger as the maximum vertical velocity increases. According to Fig. 14, it is observed that the relationship between the maximum vertical velocity and lift force is not linear. Therefore, the conventional transfer function approach based on linear relation is not applicable to the assessment of hydrodynamic load on the foil. To handle with the nonlinearity in the calculation of design load or fatigue damage, more advanced stochastic methods need to be adopted.

2.4. Comparison between local and global model

For a calculation of ultimate strength or fatigue damage of a hydrofoil in a probabilistic way, an accurate assessment of hydrodynamic force is essential, and CFD analysis is not avoidable. However, CFD analysis is quite hard and time consuming in design stage. Therefore, it would be beneficial to use a simple local model instead of 3D entire model as long as the results between them are not different significantly. The feasibility is investigated by comparing the three models defined above. 3D effect which is caused by the vortex occurring at the end of foil span is examined by comparing the hydrodynamic loads of 2D model (Model I) with 3D model (Model II). The effect of the existence of hull form is investigated by identifying the difference between 3D model with simple wall (Model II) and 3D model with hull form (Model III). The results of the comparison of lift coefficients are described in Fig.15. Max. Vertical velocity is fixed 12.57m/s, and inlet flow velocity ranges from 8.0 m/s to 14.0 m/s.

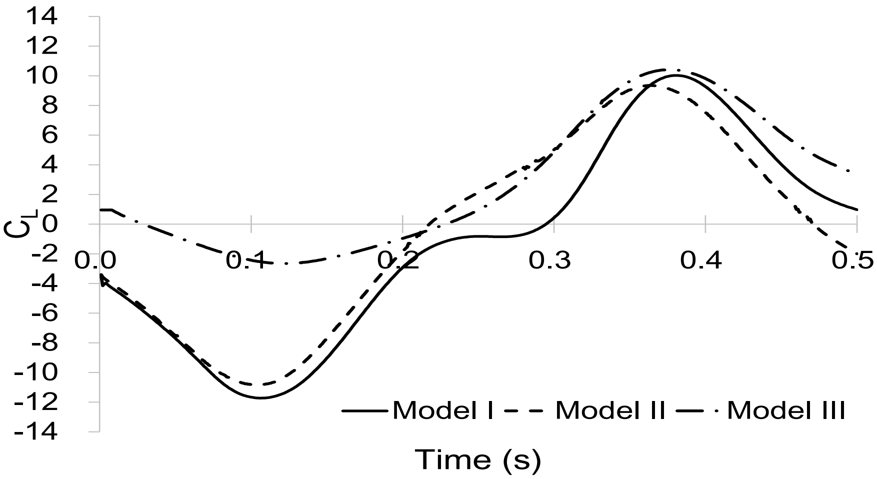

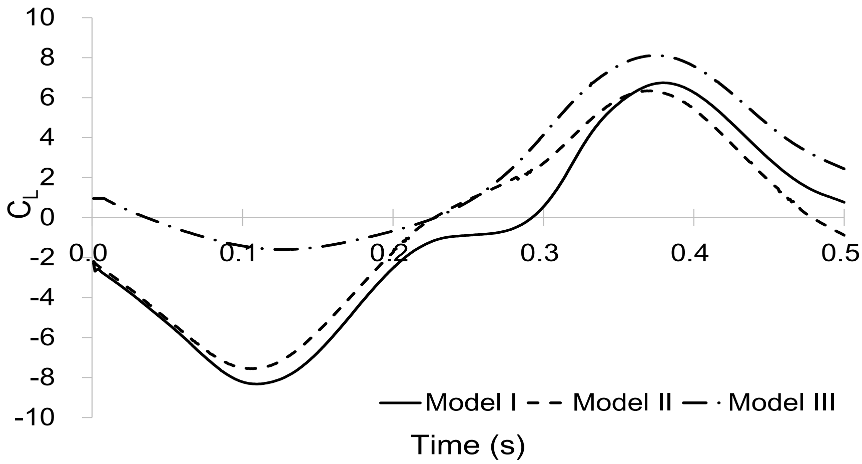

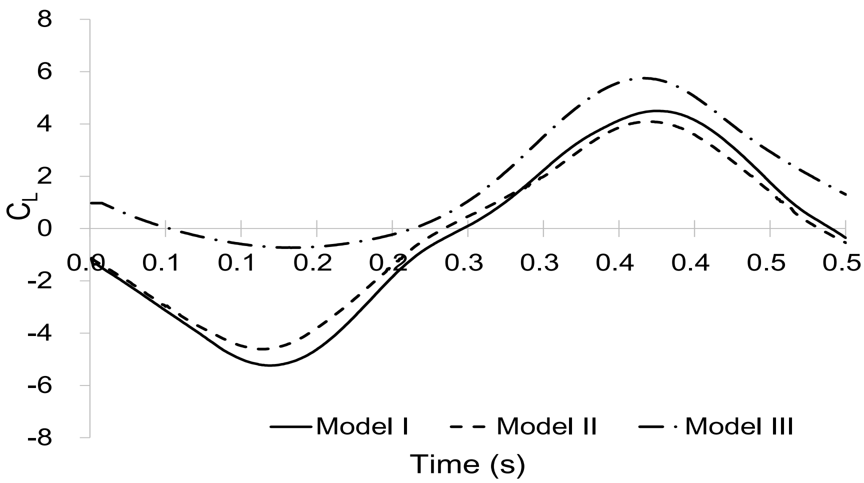

Fig 15 Comparison of lift coefficient 8.0 vs 10.0 vs 14.0 (m/s)

Fig.16 shows that the lift coefficients calculated based on model I and II are not much different. The difference between two results is approximately 10%. This similarity between model I and II describes that downwash effect induced vertical velocity by trailing vortex system does not affect considerably to hydrodynamic force in this simulation. However, model III shows significant difference comparing to the result of model I and II because the hull form of the ship causes the change of inlet flow direction. Fig. 17 shows that the direction of inlet flow is not parallel to that of the hydrofoil. Since the angle of attack is inclined upward, lift force is canceled when the foil moves upward. On the other hand, the lift force is doubled when the hydrofoil goes downward.

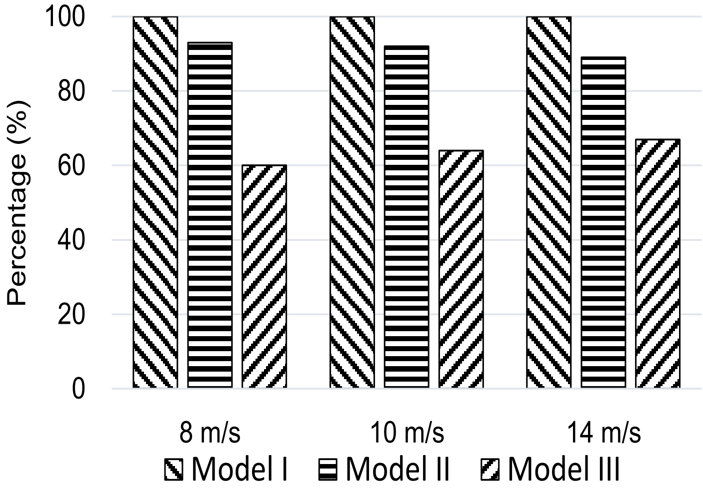

Fig 16 Comparison of lift coefficient

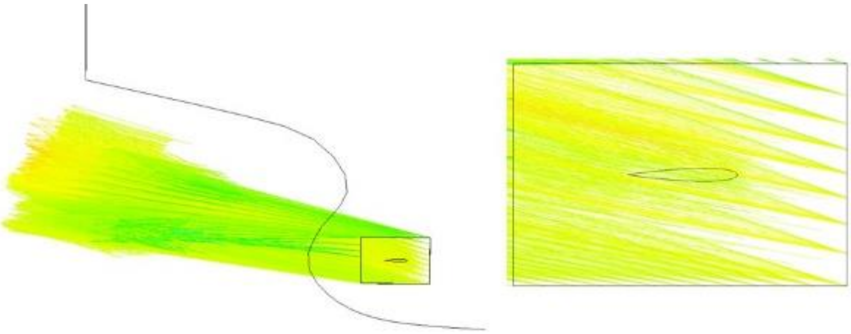

Fig 17 Streamline in steady state (U=10.0m/s)

3. Comparison of hydrodynamic analysis with CFD analysis

3.1. Hydrodynamic analysis of container ship

Motion analysis for full load condition of the container ship under irregular wave is performed in time domain using DNV.WASIM. Transfer functions of 6 DOF motions are calculated through a fast fourier transform (FFT) for the time domain analysis results. Data required for the motion analysis are as follows.

1) Hydrodynamic model of container ship

2) Loading condition and light weight information

3) Damping coefficient and information for motion control spring

Table 2, Table 3, and Table 4 summarize each item used in the motion analysis. Although full speed of ship is 24 knots, ship speed used in the analysis is 2/3 of full speed, 16 knots, as recommended for ULS (Ultimate Limit State) condition and FLS (Fatigue Limit State) by DNV CN 30.7 & 34.1 [3, 4] . Motion control springs are used for controlling surge, sway and yaw motion. For a critical damping matrix, only roll damping coefficient is applied.

Table 2 Main dimensions of container ship

Capacity [TEU]	LOA [m]	Breadth [m]	Depth [m]	Speed [knots]
10,000	330.9	48.4	27.6	24

Table 3 Mass information of container ship – HOMO.LOAD SCANT (14MT/TEU, 7,688 TEU)

<table>
<tr><th colspan="2">Displacement [ton]</th><th>Draft [m]</th></tr>
<tr><td colspan="2">149,817</td><td>13.98</td></tr>
<tr><th colspan="3">COG [m]</th></tr>
<tr><td>X</td><td>Y</td><td>Z</td></tr>
<tr><td>153.73</td><td>0</td><td>21.73</td></tr>
<tr><th colspan="3">COB [m]</th></tr>
<tr><td>X</td><td>Y</td><td>Z</td></tr>
<tr><td>153.18</td><td>0</td><td>7.84</td></tr>
<tr><th colspan="3">Radius of gyration [m]</th></tr>
<tr><td>X</td><td>Y</td><td>Z</td></tr>
<tr><td>15.63</td><td>74.33</td><td>75.41</td></tr>
</table>

Table 4 Information of motion control spring

	Eigen periods [s]	Damping coefficient
Surge	100	0.05
Sway	70	0.05
Yaw	70	0.05

Hydrodynamic panel model in WASIM is shown in Fig. 18.

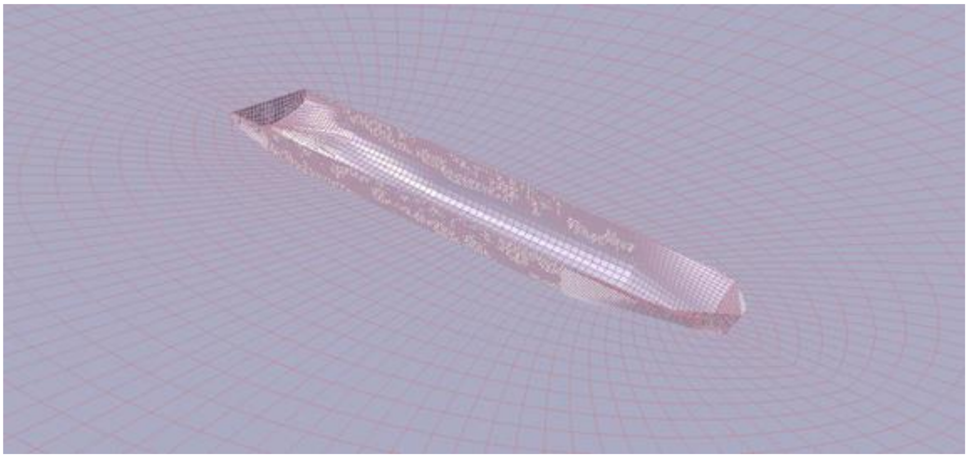

Fig 18 Hydrodynamic panel model in WASIM

By substituting velocities in heave and pitch motion at COG, vertical velocity at ESD can be calculated. Response amplitude operators (RAOs) of vertical velocity at ESD are shown in Fig. 19.

$V_{ESD} = V_{heave\ at\ COG} + l \times \tan(\dot{\theta}_{pitch\ at\ COG})$ (l : length between COG and ESD)

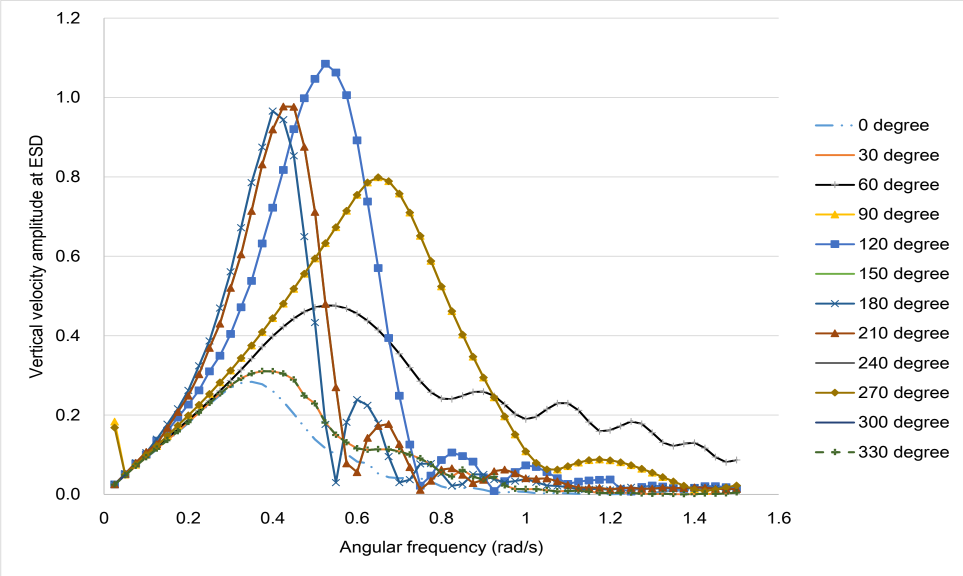

Fig 19 Vertical velocity RAOs at different wave headings

Long−term value of vertical velocity is calculated using vertical velocity RAO at ESD and wave scatter data of worldwide [5] . Data required for long−term analysis are listed below. Table 5 shows long−term values of vertical velocity of ESD at 10^{-4} &10^{-8} probability level.

1) Wave scatter data: Worldwide trade

2) Speed of ship: 8.23 m/s (16 knots)

3) Wave spectrum: PM spectrum

4) Wave directional probability: 1/12 (equally distributed at intervals of 30 degree)

5) Wave spreading function: $\cos^2$ function

Table 5 Long-term values of ESD vertical velocity

ESD vertical velocity at each probability level	
10^{-4} [m/s]	10^{-8} [m/s]
3.89	8.61

For a verification of the motion analysis results, a comparison between heave motion RAO of WADAM and WASIM is made.

Because ship speed cannot be taken into account in WADAM, heave RAOs at ship speed of 0 m/s are compared. The heave RAOs of WADAM and WASIM for head sea are plotted in Fig. 20. The overall shape of heave RAOs are nearly the same.

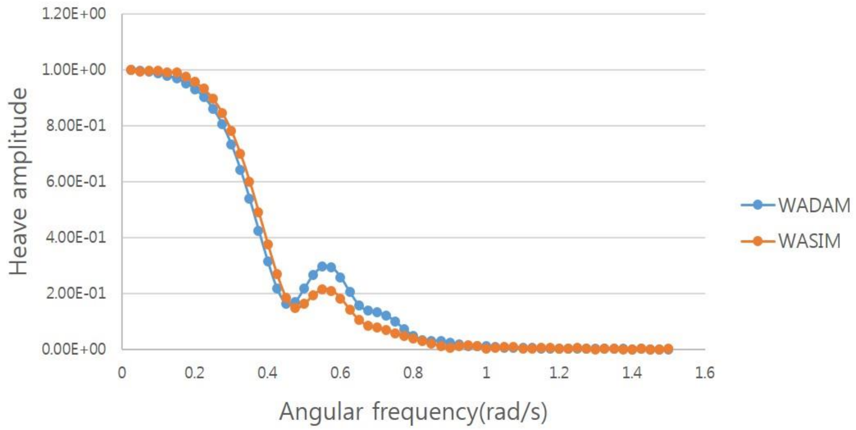

Fig 20 Comparison between heave motion RAO of WADAM and WASIM

3.2. Determination of design wave

For a verification of motion analysis in CFD using Star CCM+, CFD motion analysis results for regular wave are compared with those of WASIM. Details of CFD analysis is addressed in Section 4. For this comparison, regular wave is determined using design wave approach. Regular waves with head sea are determined such that the motion under the regular wave yields the long−term heave values at 10^{-4} &10^{-8} probability level. Frequency corresponding to peak RAO of the vertical velocity at ESD is selected and the amplitude of regular wave is defined as a ratio of long−term value to peak RAO value as below equation.

$$\text{Amplitude} = \frac{V_{\text{long-term}}}{\text{peak RAO}}$$

The frequency of peak RAO is 0.4 rad/s and peak RAO value is 0.966. The regular waves are defined in Table 6.

Table 6 Design wave amplitudes

Probability level	Amplitude	Frequency
10^{-4}	4.03 m	0.4 rad/s
10^{-8}	8.91 m	0.4 rad/s

3.3. CFD computation with VOF and DFBI

Three simplified models, model I, II and III have been treated. However, these models could not take into account the free surface effect and interaction between ship and fluid. For a more accurate calculation, DFBI(Dynamic Fluid Body Interaction) and VOF(Volume of Fluid) method are used to consider the free surface effect and the interaction between ship and fluid [6]. Star CCM+, a commercial CFD software, is used for this simulation. The model size is 1,560m (L) × 660m (B) × 700m (D). 5th order-stokes wave is generated. Trimmed mesh consisting of about 2.1 million cells is generated for the entire solution domain. To capture the fluid dynamics around the ship and hydrofoil, y+ is kept under 40 using prism layer. The overall view of the mesh around the ship is shown in Fig. 21.

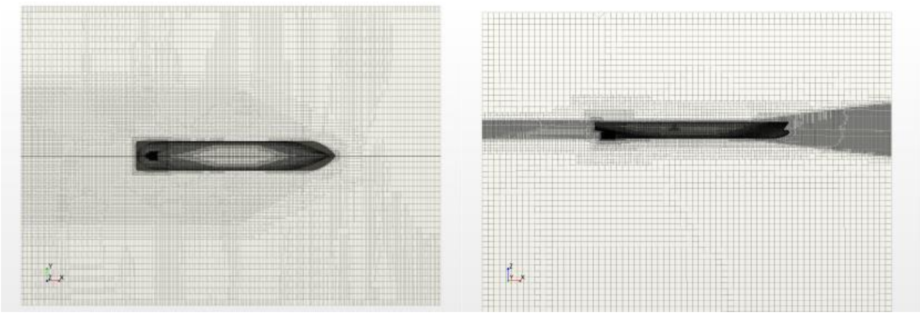

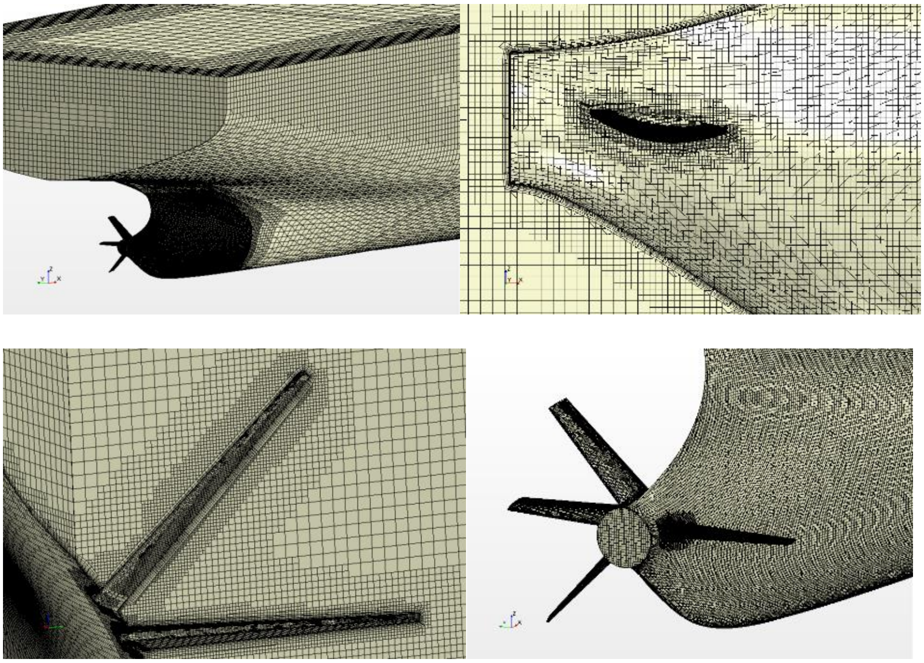

Fig 21 Overall view of the mesh around the ship of CFD model

In order to consider ship speed effect, forward speed of 8.23 m/s is assigned to ship. Sufficient large space is included at stern side and damping zone of 1.0L (330m) is applied to the outlet boundary to reduce wave oscillation near outlet boundary. The damping zone prevents the reflected wave from disturbing the input regular wave. This enable to keep the same wave height at the vessel location. Fig. 22 illustrates CFD calculation results.

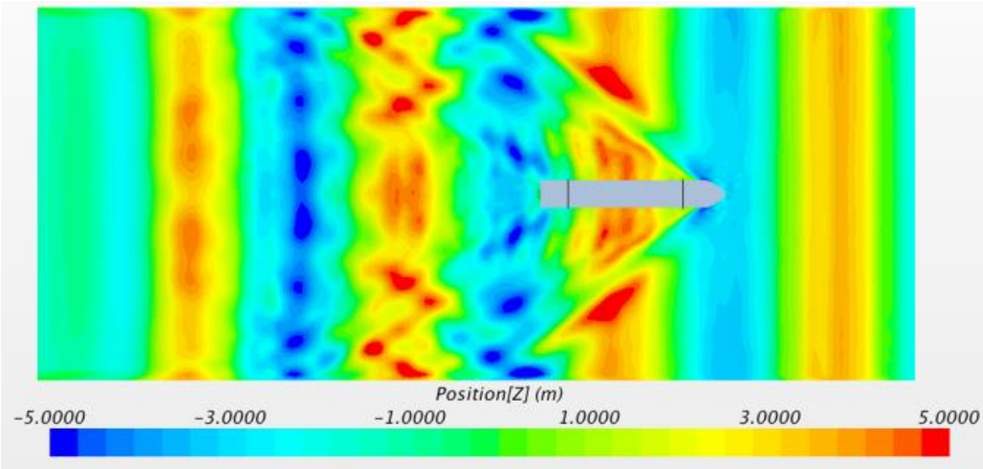

Fig 22 CFD model analysis results for regular wave

3.4. Comparison of CFD calculation and WASIM results

Heave and pitch motions under the regular waves of head sea defined in Table 6 are compared in Fig. 23 and Fig. 24. It can be regarded they show a considerably good agreement. Difference in heave motion is slightly larger than that of pitch motion. The reason of difference in heave motion can be explained by the sensitivity of heave motion at the period of the regular waves, 15.71 s (angular frequency = 0.4 rad/s). Fig. 25 and Fig. 26 illustrate the heave RAO values is considerably sensitive to ship speed. However, the lifting force is mainly affected by vertical velocity at ESD and the contribution of pitch to the vertical velocity is much larger than heave motion. Therefore, the vertical velocities at ESD from CFD analysis and WASIM analysis matches well as shown in Fig. 27 and Fig. 28.

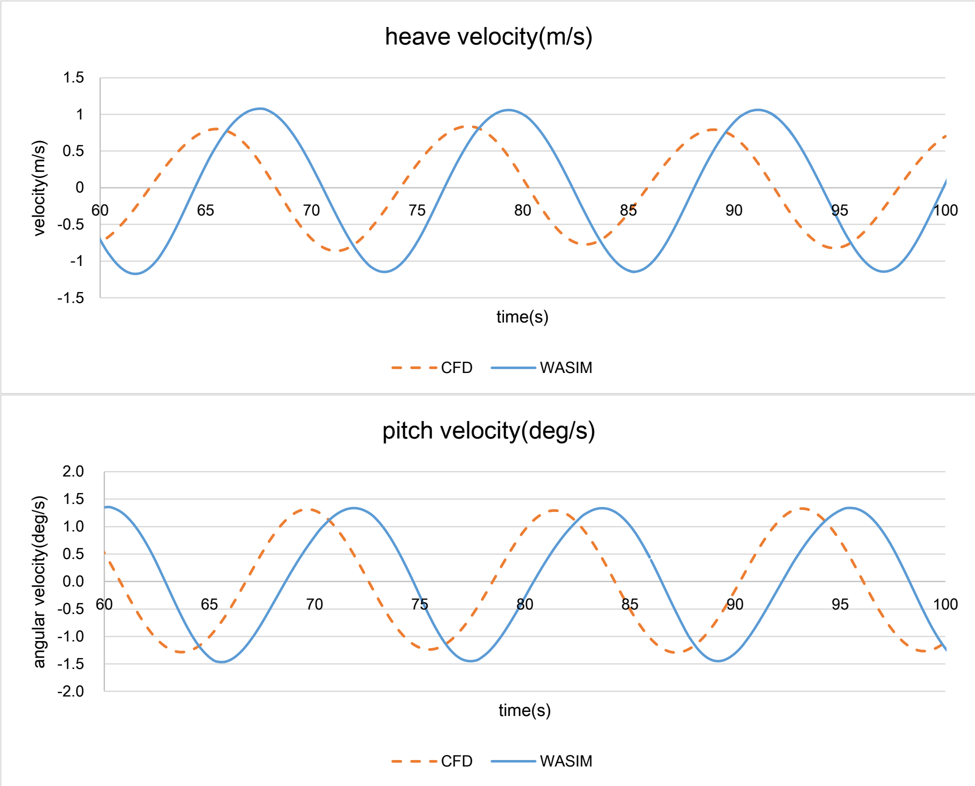

Fig 23 Comparison of heave & pitch motion for regular wave of head sea with 10^{-4} probability

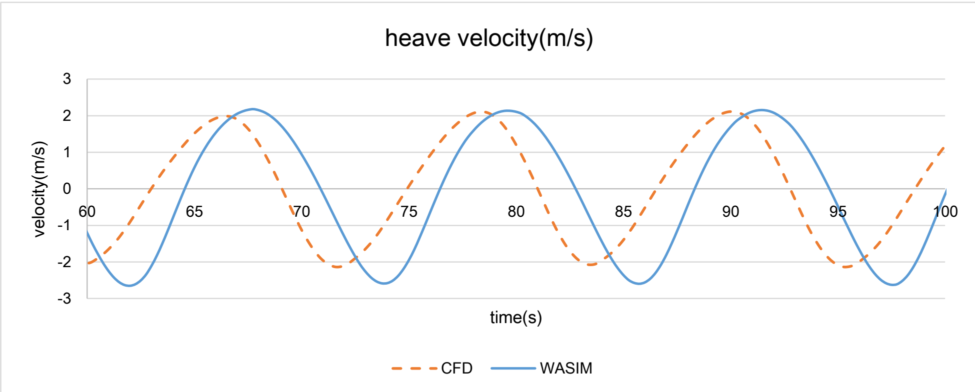

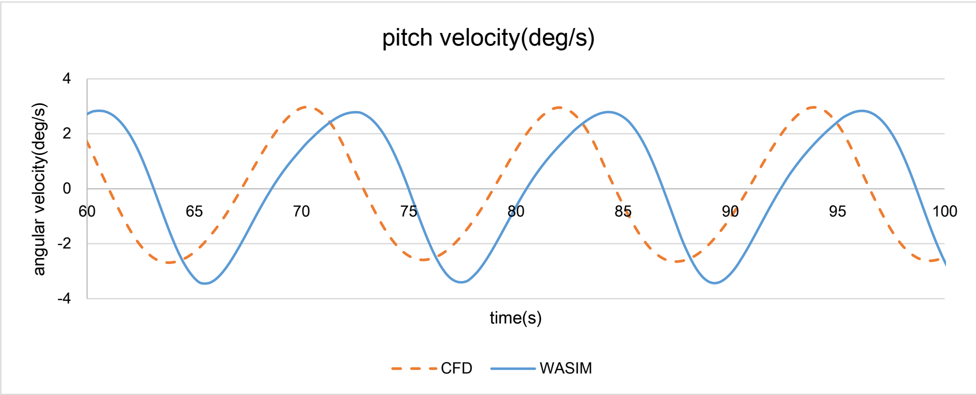

Fig 24 Comparison of heave & pitch motion for regular wave of head sea with 10^{-8} probability

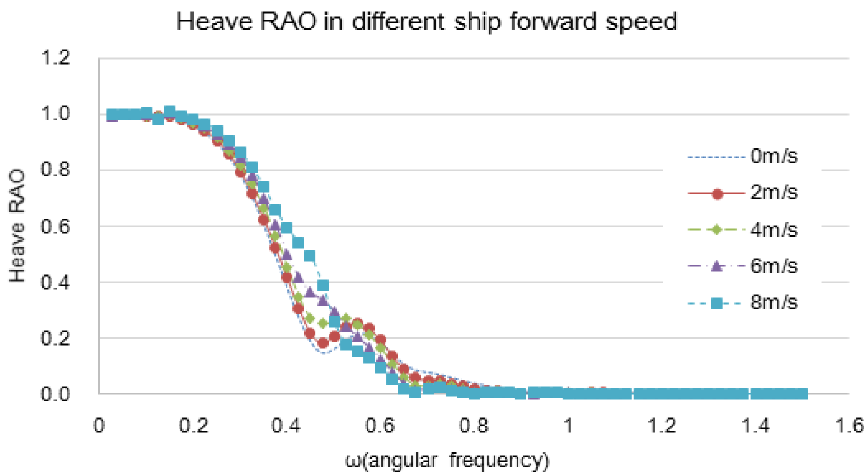

Fig 25 Heave RAO for different ship speeds

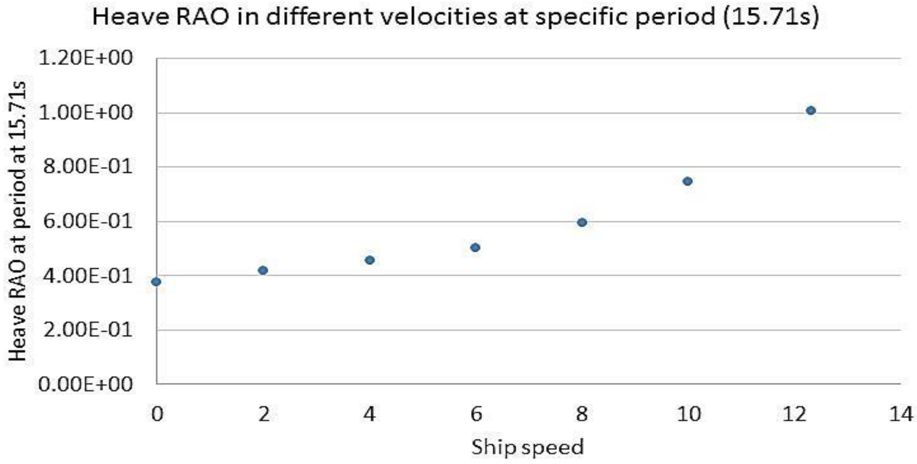

Fig 26 Variation of heave RAO values for different ship speeds

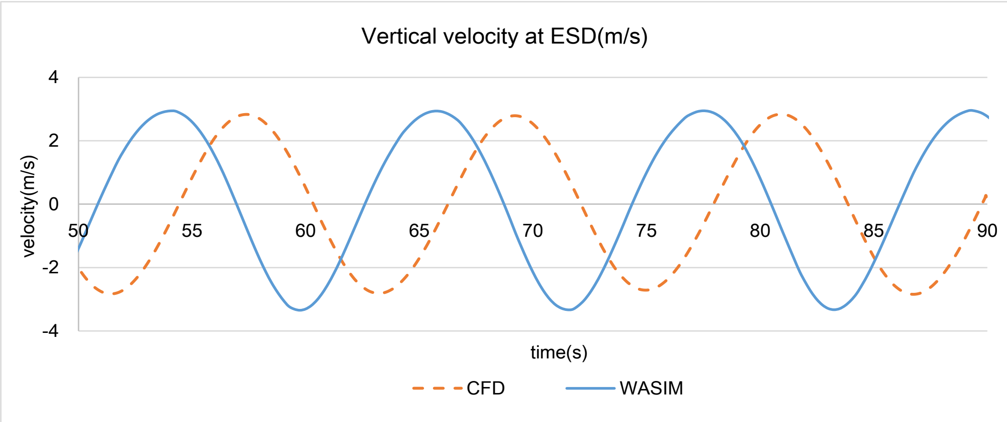

Fig 27 Comparison of vertical velocities at ESD for a regular wave of head sea with 10^{-4} probability

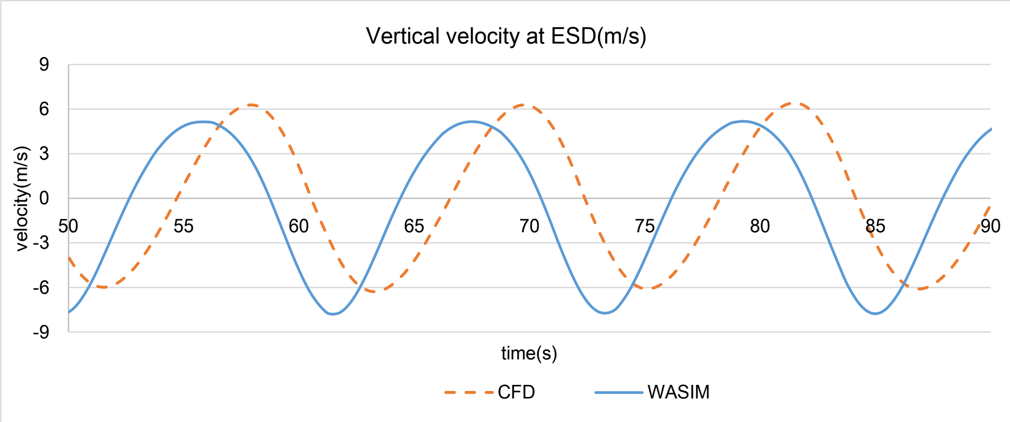

Fig 28 Comparison of vertical velocities at ESD for a regular wave of head sea with 10^{-8} probability

For regular waves of quartering and beam sea, heave, pitch and ESD motion are compared in Fig. 29 and 30. In case of quartering sea, the result of heave,pitch and vertical velocity at ESD match well. However, the pitch difference in beam sea looks larger than that in head and quartering sea. The magnitude of pitch velocity in beam sea is 0.1 (deg/s) and it is only 10 % of quartering sea. Besides, in this beam sea, the heave is governing to the vertical velocity.

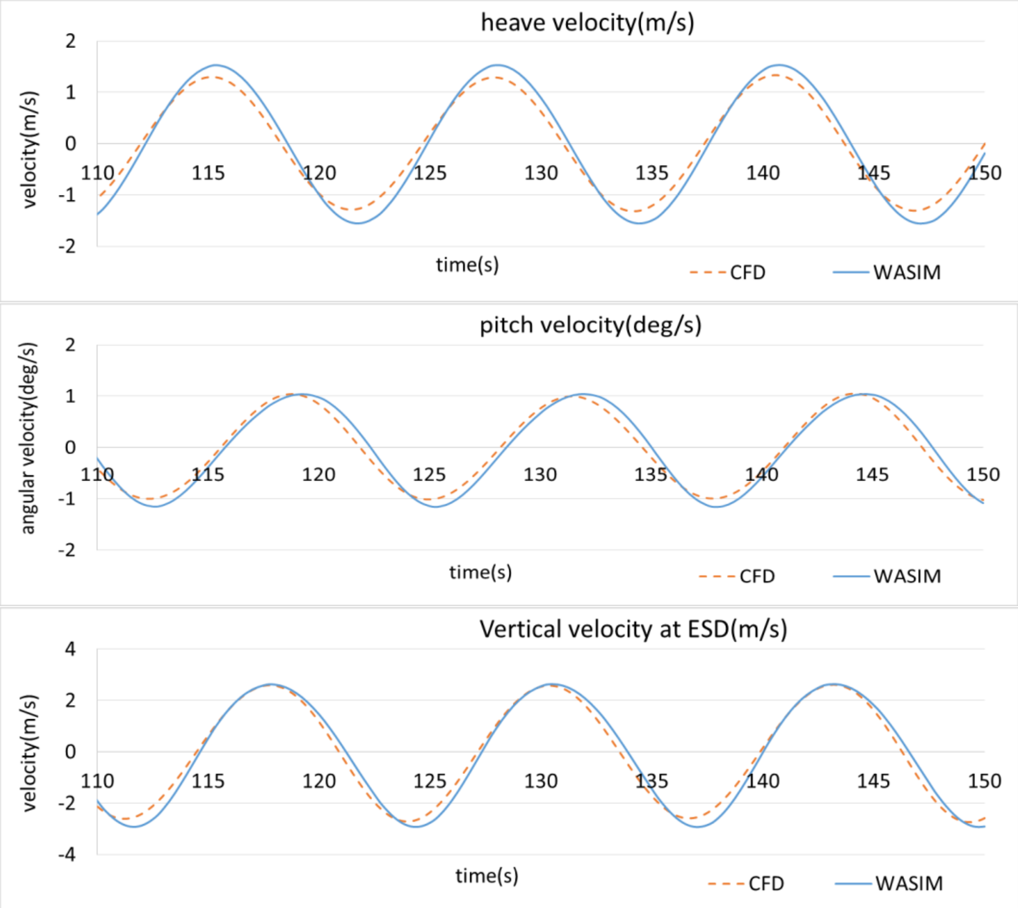

Fig 29 Comparison of haeve, pitch and vertical velocities at ESD for a regular wave of quartering sea with 10^{-4} probability

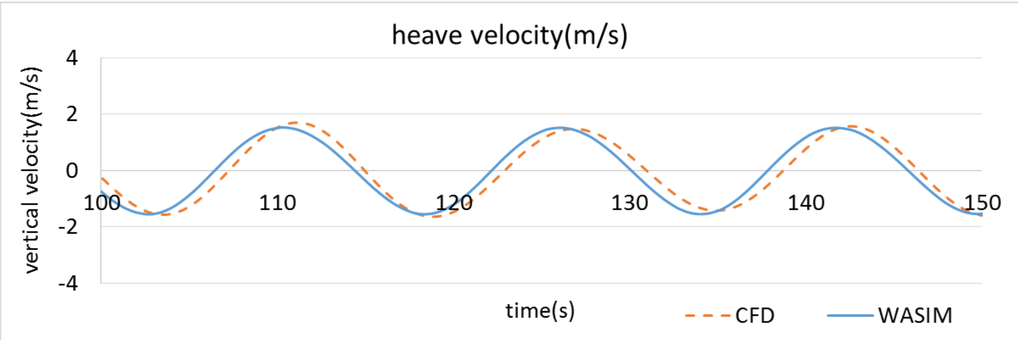

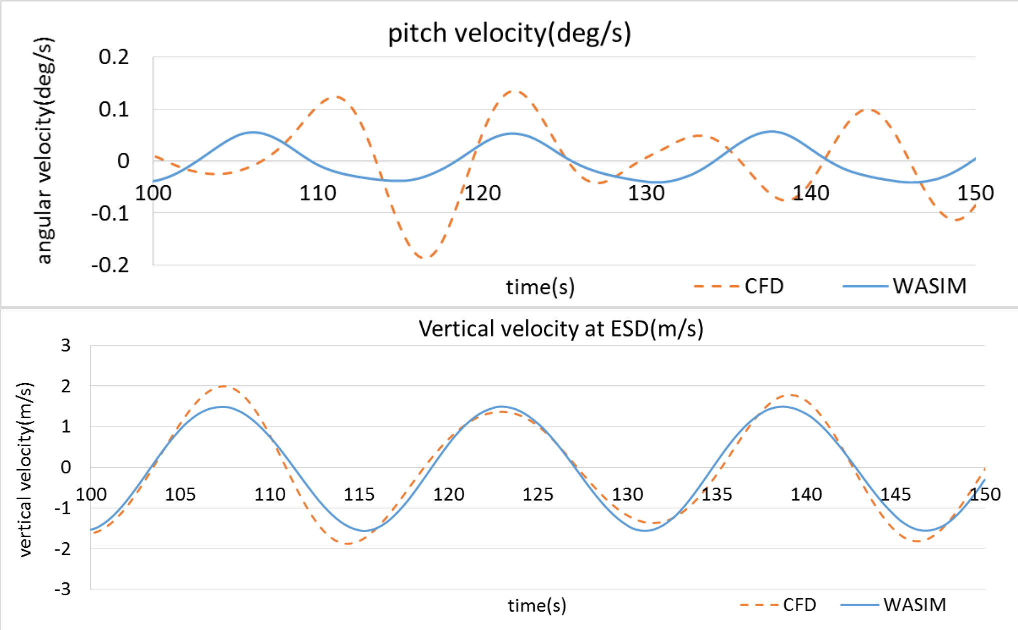

Fig 30 Comparison of haeve, pitch and vertical velocities at ESD for a regular wave of beam sea with 10^{-4} probability

4. Calculation of loads on ESD

In the previous section, ship motion analysis using CFD analysis was addressed. This section describes the calculation of loads on ESD using CFD analysis.

4.1. Effect of different periods to hydrodynamic force

In this section, the effects of different periods of vertical velocity at ESD are investigated. To identify the most dominant period range for vertical velocity, its response spectrums for all sea states with Hs=4m are calculated using frequency domain analysis using DNV.WASIM. The response spectrum are cumulated Finally, the results are cumulated. The illustration of the procedure is also shown in Fig. 31. The most dominant period ranges from 13(s) to 17(s).

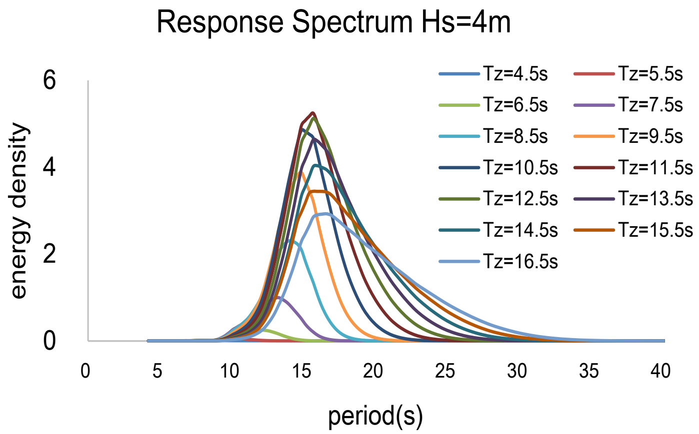

(a) vertical velocity response spectrum

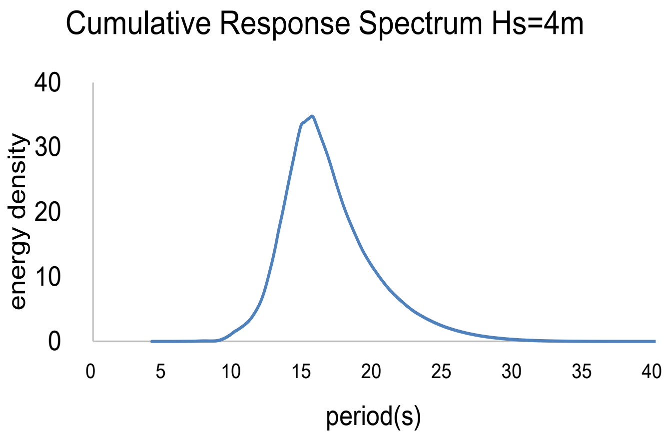

(b) cumulative energy density

Fig 31 Dominant period range of vertical velocity

Based on the above result, CFD analysis using Model III (3D model with hull form) is performed to identify the effect of the different period of vertical velocity at ESD. The vertical velocity profiles shown in Fig. 32 are applied to Model III. Free surface effect is not taken account. The results are shown in Fig.33 and Table 7.

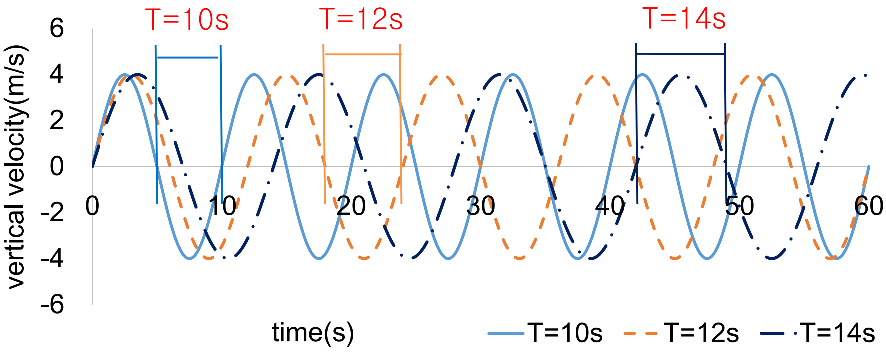

Fig 32 Different periods of vertical motion

Table 7 C_L vs period of vertical motion

Vertical velocity	C_L	Period					average
		11s	12s	13s	14s	15s	
2.5m/s	Max	2.12	2.15	2.13	2.09	1.89	2.08
	Min	−2.02	−2.18	−2.14	−2.10	−1.72	−2.03
3.5m/s	Max	2.03	1.88	1.63	1.32	1.05	1.58
	Min	−2.58	−2.45	−2.22	−1.96	−1.62	−2.17
4.5m/s	Max	1.35	1.52	1.63	0.99	1.75	1.47
	Min	−2.30	−1.96	−1.63	−1.05	−1.18	−1.45

From these results, hydrodynamic load on ESD is affected by the periods of vertical velocity even if the magnitude of the velocity is the same. Therefore, it is necessary to consider the period of vertical velocity for the estimation of hydrodynamic load on the ESD.

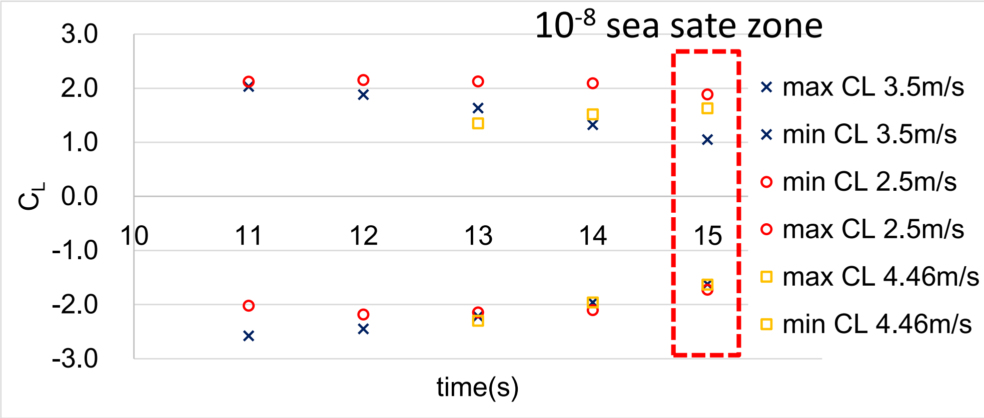

Fig 33 C_L v.s. period of vertical motion in 3D CFD Model

4.2. Estimation of hydrodynamic force using global model

4.2.1. Calculation of loads on ESD using CFD analysis

In order to quantify the load on ESD, a local coordinate is created at the root of ESD as shown in Fig. 34 and shear force and vertical bending moment at the root is calculated by integrating the pressure on the ESD. Fig. 35 shows shear force and bending moment at four ESDs under a regular wave of 10^{-8} probability. The frequency of the forces is similar to wave encounter frequency.

ESD No.3 is found to experience the largest shear force and bending moment. Thus, EDS No. 3 is selected for further calculation for long term analysis and strength assessment.

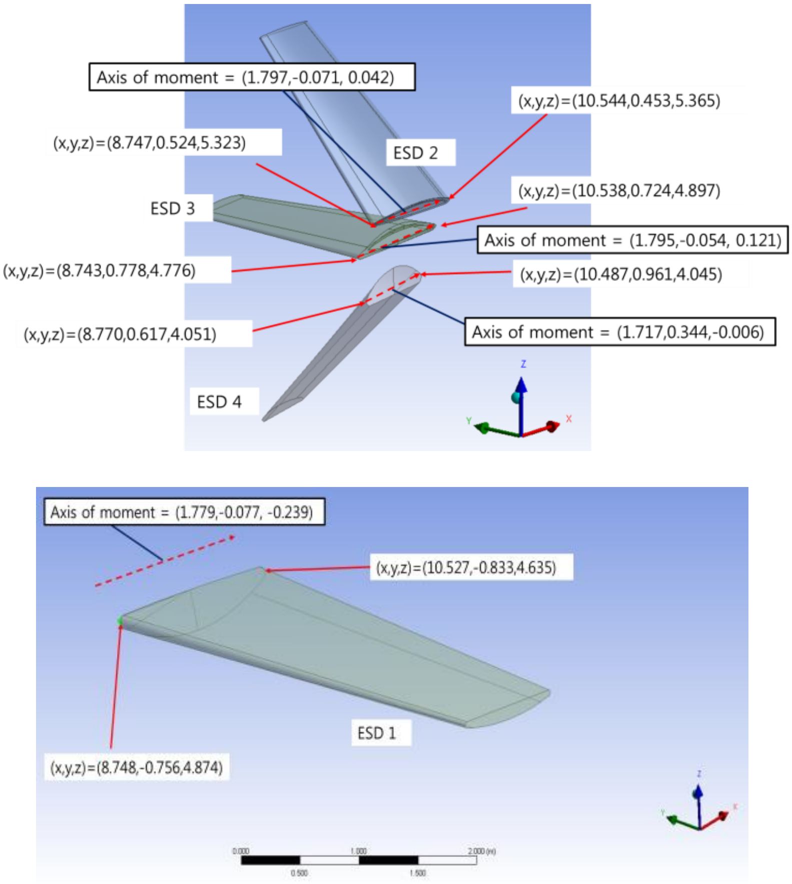

Fig 34 Definition of local coordinates at the root of ESDs

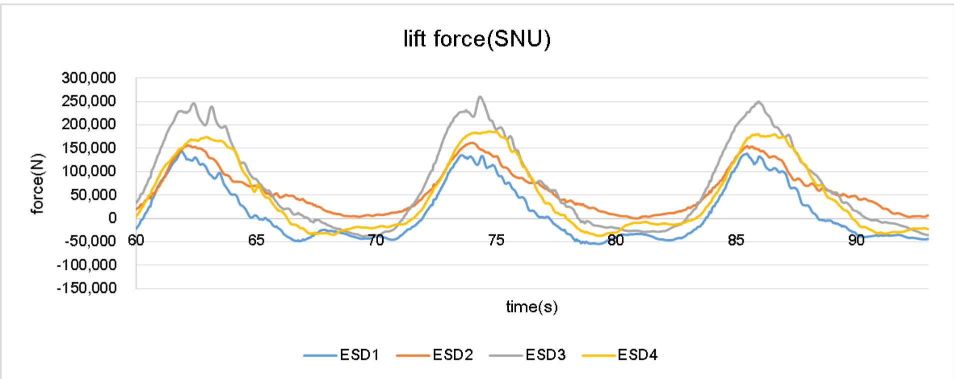

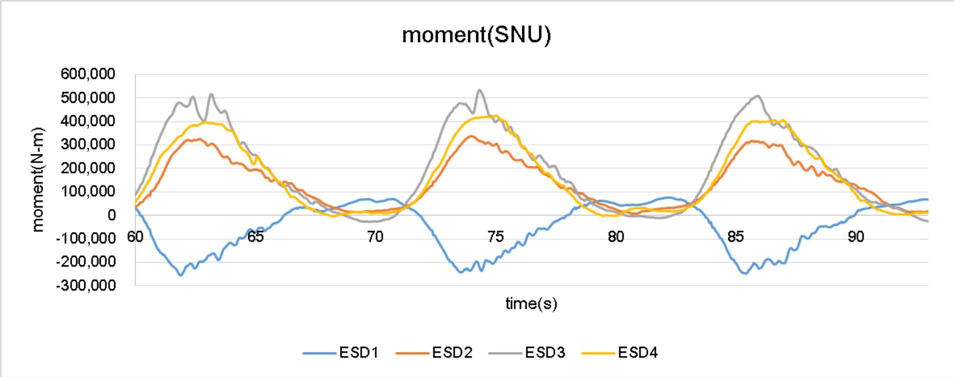

Fig 35 Vertical lifting force and movement at ESDs for a regular wave of 10^{-8} probability

4.2.2. Prediction of the magnitude and period of vertical velocity at ESD

For the estimation of hydrodynamic force on ESD, CFD analysis requires excessive time and cost. Therefore, it is essential to find an efficient method. This research proposes neural network to approximate the hydrodynamic forces as a function of magnitude and frequency of the vertical velocity.

Firstly, Sea-keeping analysis is performed to identify the bounds of magnitude and period of vertical velocity at ESD prior to CFD analysis. The period is found to range from 0(s) to 36(s) and the magnitude from 0 (m/s) to 10(m/s). Then, a set of uniformly distributed regular waves are generated and a series of CFD calculations are performed for the waves.

4.2.3. CFD analysis for sample data

In previous step, the bounds of the magnitude and periods of vertical velocity are determined. A series of CFD analysis are performed for total 58 regular waves listed in Table 8. Initially, WASIM analyses for uniformly distributed regular waves are performed and the resultant vertical velocities and periods are plotted in a graph. However, the data is not uniformly distributed. Periods are uniformly distributed since it follows the frequency of the incoming wave. However, the magnitudes are not since it is determined by multiplying wave height to RAO value. Therefore, the uniformly distributed regular wave data are adjusted such that the resultant velocity data are not clustered as much as possible. In this research, only head sea is considered for a convenience of CFD computation.

Table 8 Regular waves used for CFD analysis

No	H(m)	T(s)	No	H(m)	T(s)	No	H(m)	T(s)
1	2	18	21	10	24	41	20	16
2	3	26	22	10	22	42	20	18
3	3	30	23	11	13	43	20	20
4	4	18	24	12	12	44	20	22
5	4	24	25	12	16	45	20	24

6	4	30	26	12	14	46	20	26
7	4	17	27	12	18	47	22	14
8	5	16	28	12	20	48	22	16
9	5	30	29	13	13	49	22	18
10	6	14	30	14	12	50	22	20
11	6	20	31	16	14	51	24	14
12	6	28	32	16	16	52	24	16
13	6	17	33	16	18	53	24	18
14	7	14	34	16	20	54	24	20
15	7	16	35	16	22	55	26	14
16	8	18	36	16	16	56	26	16
17	8	16	37	18	14	57	26	18
18	9	30	38	18	16	58	26	20
19	9	20	39	18	18			
20	9	17	40	20	14			

The resultant period and amplitudes of vertical velocities at ESD No. 3 are plotted in Fig.36 and Table 9. The data are not distributed across the entire area. The shape is similar to RAO shape of vertical velocity. That is, for high and low periods, the corresponding transfer function is small. Thus, the resultant velocity is small even if the wave height of incoming wave is large.

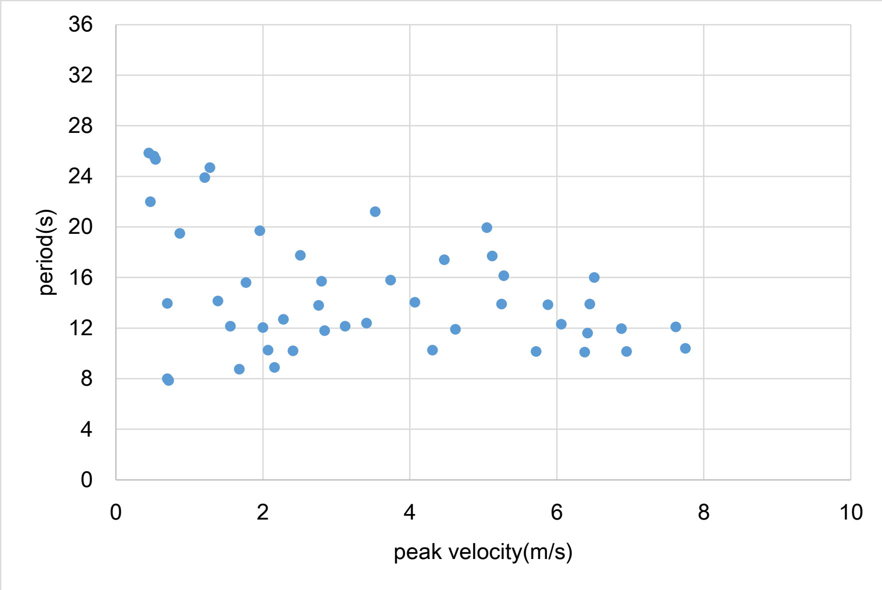

Fig 36 Resultant periods and peak velocities from CFD analysis for regular waves

Table 9 Resultant periods and peak velocities

No	Peak vel (m/s)	period(s)	No	Peak vel (m/s)	period(s)	No	Peak vel (m/s)	period(s)
1	0.45	25.85	21	2.51	17.75	41	6.42	11.60
2	0.47	22.00	22	2.76	13.80	42	6.45	13.90
3	0.52	25.60	23	2.80	15.70	43	6.51	16.00
4	0.54	25.35	24	2.84	11.80	44	6.88	11.95
5	0.70	13.95	25	3.12	12.15	45	6.95	10.15
6	0.70	8.00	26	3.41	12.40	46	7.12	15.95
7	0.72	7.85	27	3.53	21.20	47	7.40	13.76
8	0.87	19.50	28	3.74	15.80	48	7.52	10.35
9	1.21	23.90	29	4.07	14.05	49	7.62	12.10
10	1.28	24.70	30	4.31	10.25	50	7.75	10.40
11	1.39	14.15	31	4.47	17.40	51	7.87	15.85
12	1.56	12.15	32	4.62	11.90	52	8.05	14.10
13	1.68	8.75	33	5.05	19.95	53	8.33	12.10
14	1.77	15.60	34	5.12	17.70	54	8.61	16.05

15	1.96	19.70	35	5.25	13.90	55	8.76	14.05
16	2.00	12.05	36	5.28	16.15	56	8.81	10.50
17	2.07	10.25	37	5.72	10.15	57	8.89	12.15
18	2.16	8.90	38	5.88	13.85	58	9.40	12.15
19	2.28	12.70	39	6.06	12.30			
20	2.41	10.20	40	6.38	10.10			

4.2.4. Training of neural network for loads on ESD

From the above sample positions, lift force and moment data of ESD No. 3 are calculated from CFD analysis and the data are used to train neural network. Neural network is known as a powerful data modeling tool and it is able to capture and represent input and output relationships well. The number of input, output and hidden nodes are 2, 2 and 5, respectively. Tangent sigmoid is used as transfer function. The procedure of neural network is described in Fig.37.

Total 58 data are used to train the neural network and the contour lines of lifting force and bending moment are shown in Fig. 38 and 39. The approximated area is limited to the area where vertical velocity profile actually exist.

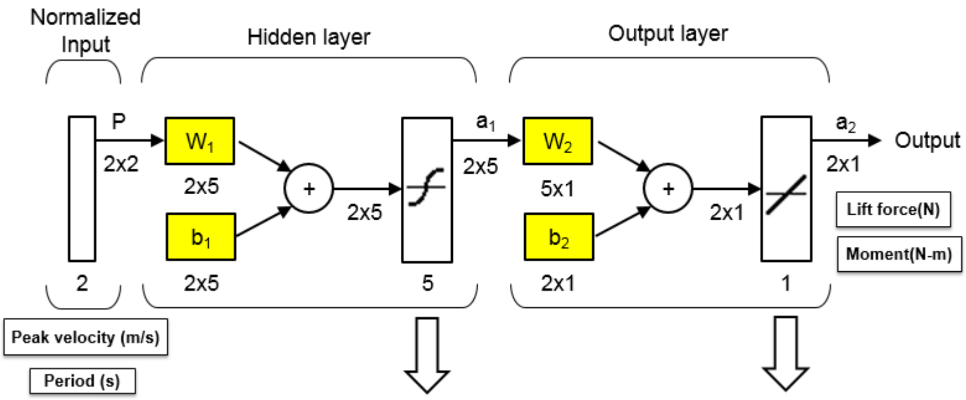

$$a_1 = tansig(P \times W_1 + b_1) \qquad a_2 = purelin(a_1 \times W_2 + b_2)$$

$$tansig(x) = \frac{e^{2x} - 1}{e^{2x} + 1} \qquad purelin(x) = x$$

Fig 37 Procedure of neural network

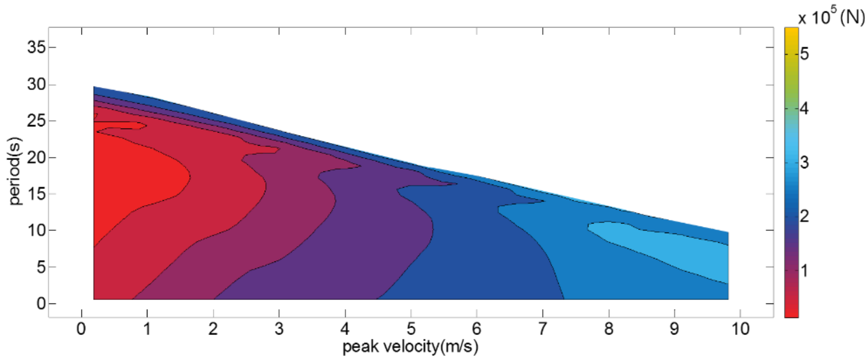

Fig 38 Contour line of lift force

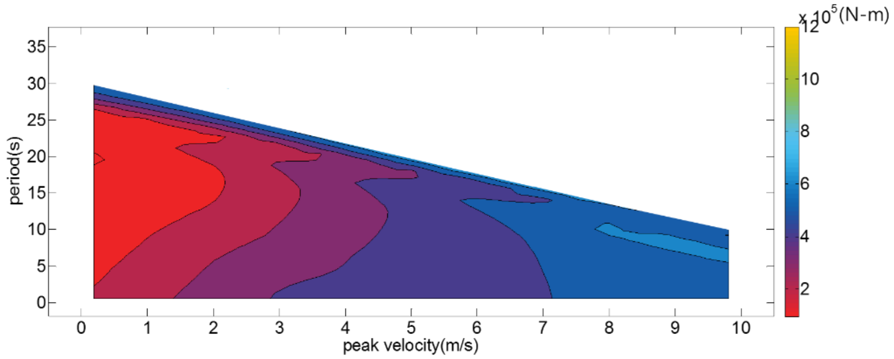

Fig 39 Contour line of moment

4.2.5. Heading angle effect on hydrodynamic force

To investigate the effect of heading angle on hydrodynamic force, the sample data with the same vertical velocity, period and different heading angles are generated.

In the first step, the relation between encounter frequency of wave and frequency of vertical velocity at ESD is used. As shown in Fig. 40, the correlation equation is almost linear. Therefore, from the target period at ESD, encounter frequency of wave can be calculated.

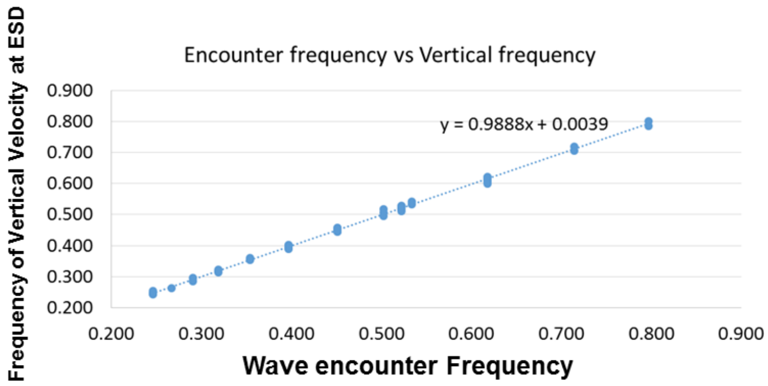

Fig 40 Correlation equation between frequency of wave and ESD

Then, RAO of vertical velocity at the frequency of wave can be used to calculate a height of wave to be applied the simulation. The detail of procedure is described in Fig.41.

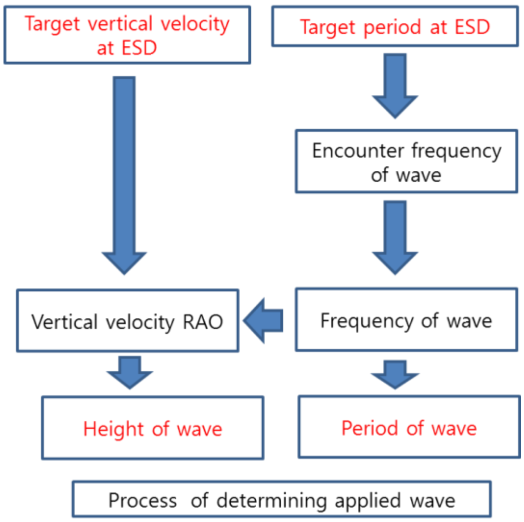

Fig 41 Procedure to determine wave height and period for simulation

The resultant lift forces and moments from the sample are plotted in Fig.42. Almost resultant lift forces and moments from head sea are larger than that from quartering and beam sea. The reason is that larger relative encounter speed in head sea makes larger inlet flow speed and particle velocity in beam and quartering sea is reduced by the effect of wave radiation. Thus, the neural network trained from the data of head sea will be used to calculate for long−term value and fatigue life as conservative way.

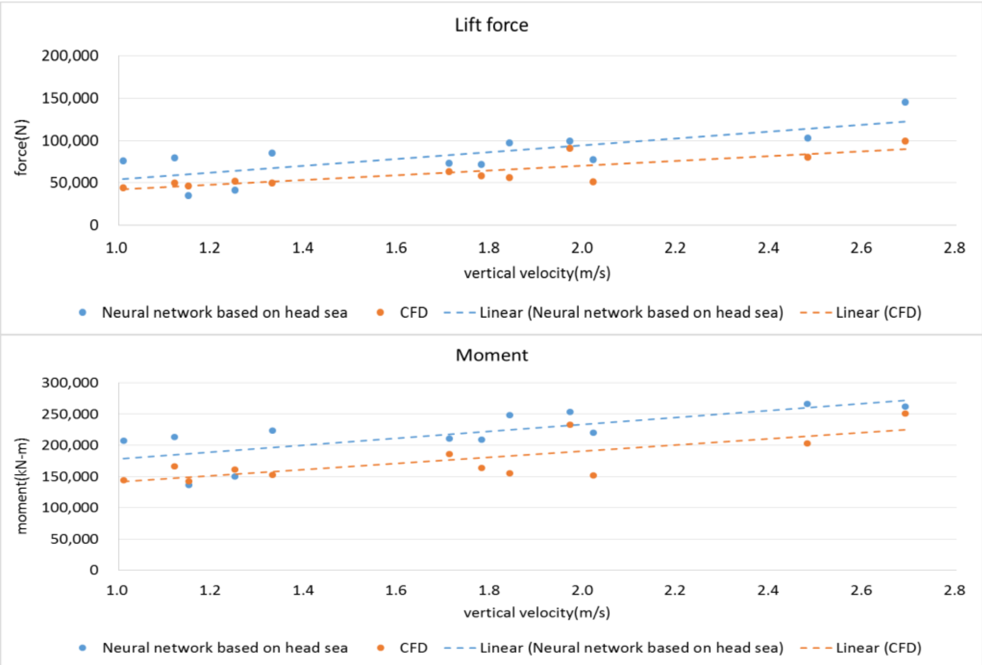

Fig 42 Resultant lift force and moment at sample data

5. Long-term analysis on ESD

5.1. Classical long-term analysis

ESD No.3 is found to experience the largest shear force and bending moment. Thus, EDS No. 3 is selected for further calculation for long term analysis and strength assessment.

5.1.1. Calculation of peak velocities for each sea states using response spectrum and inverse FFT

A vertical velocity response spectrum at head sea is calculated by combining RAO and wave spectrum. The RAO is calculated from WASIM. Then, irregular time history of vertical velocities is generated form the response spectrum using inverse fourier transform as shown in Fig. 43. In order to take into account the randomness of the irregularity, twenty different irregular time histories are generated.

Then, each time history of vertical velocity is converted to time histories of lifting force (shear force) and bending moment using the trained neural network. For each sea state, the maximum peak vertical velocities among all peaks during 3 hours are collected and

Gumbel distribution is used to fit the data.

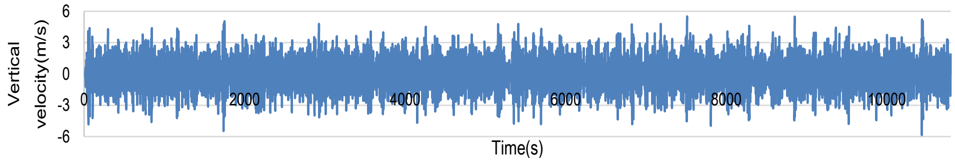

Fig 43 3 hours' time series of vertical velocity

5.1.2. Calculation of parameters of Gumbel distribution for all sea states

The parameters for Gumbel distribution are estimated from the collected peak velocities. Using the parameters, it is possible to identify the statistical characteristic of the each sea state. The Gumbel parameters for total 142 sea states are listed in Table 10.

Table 10 Gumbel parameter of lift force and moment

				Lift force		Moment	
No	Hs	Tz	probability of occurrence of a sea state defined by H_S,T_P	μ(location parameter)	σ(scale parameter)	μ(location parameter)	σ(scale parameter)
1	1	3.5	3.11E-03	-71509	93.58	-202283	193.53
2	2	3.5	2.00E-04	-71608	171.01	-202465	277.61
3	1	4.5	2.73E-02	-71738	275.46	-203114	508.59
4	2	4.5	7.64E-03	-71747	353.73	-203092	878.69
5	3	4.5	5.70E-04	-72351	759.28	-204562	1484.80
6	4	4.5	4.00E-05	-72284	796.36	-203818	1503.90
7	1	5.5	6.40E-02	-71877	418.14	-203215	738.14

8	2	5.5	4.45E-02	-72829	1014.74	-206080	2095.59
9	3	5.5	9.02E-03	-73186	1577.31	-207878	3642.58
10	4	5.5	1.50E-03	-74184	2224.07	-210723	7000.23
11	5	5.5	2.50E-04	-75529	2698.04	-213826	3978.90
12	6	5.5	4.00E-05	-73809	2641.34	-210531	6027.67
13	7	5.5	1.00E-05	-77442	4245.52	-215919	8463.96
14	1	6.5	7.13E-02	-72910	599.21	-205351	746.43
.	.	.	.	.	.	.	.
.	.	.	.	.	.	.	.
.	.	.	.	.	.	.	.
136	3	16.5	1.00E-05	-121494	59193.41	-309644	131378.96
137	4	16.5	1.00E-05	-139036	62821.00	-357395	136266.91
138	5	16.5	1.00E-05	-160445	54084.61	-411316	119510.85
139	6	16.5	1.00E-05	-170172	54193.74	-415048	119519.56
140	7	16.5	1.00E-05	-159470	41023.28	-412891	97777.61
141	8	16.5	1.00E-05	-214871	52347.54	-534351	133959.94
142	9	16.5	1.00E-05	-226729	49183.52	-546009	103110.33

Fig. 44 shows samples of Gumbel fit for maximum velocity values for a sea state, H_S=14 m and T_Z=11.5 sec. The sea state was identified to result in the largest vertical velocity value among all sea states in world−wide scatter diagram. The fitting is found to match well with the sampling data.

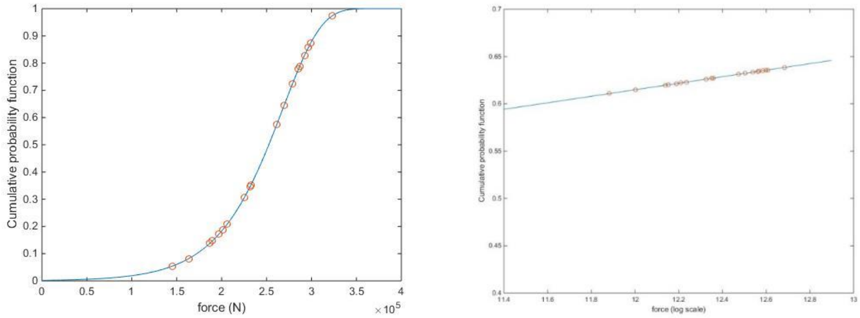

(a) Gumbel fitting for max lifting force a sea state (Hs=14 m and Tz=11.5 sec)

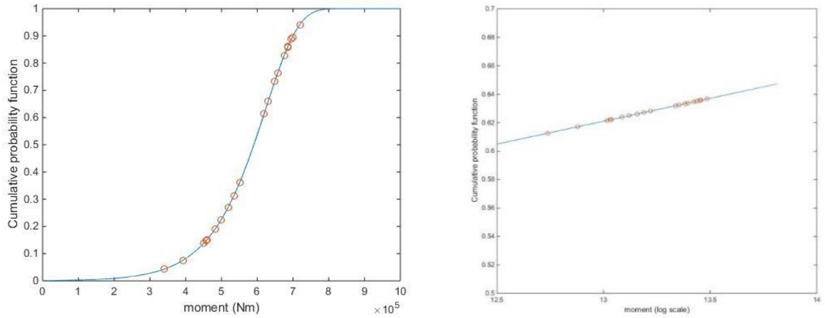

(b) Gumbel fitting for max bending moment a sea state (Hs=14 m and Tz=11.5 sec)

Fig 44 Contribution coefficient for all sea states

5.1.3. Summation of short-term probabilities of exceedance in combination with occurrence of sea states

The long term distribution equation of 3−hour maximum values is represented by

$$Q_{X_{3h}}(x) = 1 - F_{X_{3h}}(x) = \iint_{0,,0}^{\infty,\infty} \left(1 - F_{X_{3h|HsTp}}(x|h,t)\right) \cdot f_{HsTp}(h,t)dtdh$$

$Q_{X_{3h}}$: Exceedance probability of 3 hours' maximum values

Gumbel fit for 3-hour maximum distribution of all realizations for a sea state defined by (h,t)

$$F_{X_{3h|HsTp}}(x|h,t) = \exp\left\{-exp\left[-\left(\frac{x-\alpha(h,t)}{\beta(h,t)}\right)\right]\right\}$$

Joint probability density function for wave scatter data is represented by

$$f_{HsTp}(h,t) = f_{Hs}(h) f_{Tp|Hs}(t,h)$$

$f_{HsTp}(h,t)$: occurrence probability of a sea state represented by h and s.

Long term response pressure (xq) is found by

$$Q_{X_{3h}}(x_q) = 1 - F_{X_{3h}}(x_q) = \frac{q}{m_{3h}}$$

q : annual exceedance probability (=1/20 years)

m_{3h} : the annual number of short term events (=20 years×365 days × 24 hours / 3 hours)

According to the above formula, the calculated long-term value of lift force and moment considering head sea only are 338 (KN) and 677 (KN-m), respectively. Considering all heading angles, the lift force and moment are 258 (KN) and 536(KN−m), respectively.

5.2. Estimation of long-term extreme value using contribution coefficient

5.2.1. Selection of the most important sea state defined by the contribution coefficient

Normally, long−term extreme value is obtained by combining the response in all sea states [7] . The long−term value for a linear system can be effectively obtained by determining the response for each sea state in frequency domain. However, if the response is nonlinear, a time domain simulation is required to consider the nonlinear effect. However, due to the time consuming time domain analysis, it is nearly hard to run time domain hydrodynamic analysis for all sea states in wave scatter diagram. In this respect, it is very crucial to improve the efficiency of the calculation. In contribution coefficient method, it is shown that the long−term extreme can be estimated by considering only a few short−term sea states [8] .

The first step for this method is to determine the most critical sea state using the contribution coefficient. The contribution to the probability of exceedance for a sea state is given below.

$$C_R(si) = \frac{\text{short-term cumulative probability}(si) \times \text{probability of occurence}(si)}{\text{probability of exceedance}}$$

To calculate the contribution coefficient, it is used time domain based on the relation between the lifting force and vertical velocity at ESD is linear. The change even if including the nonlinear relations may be negligible. The detail of procedure to calculate the linear long−term value is described in Fig.45.

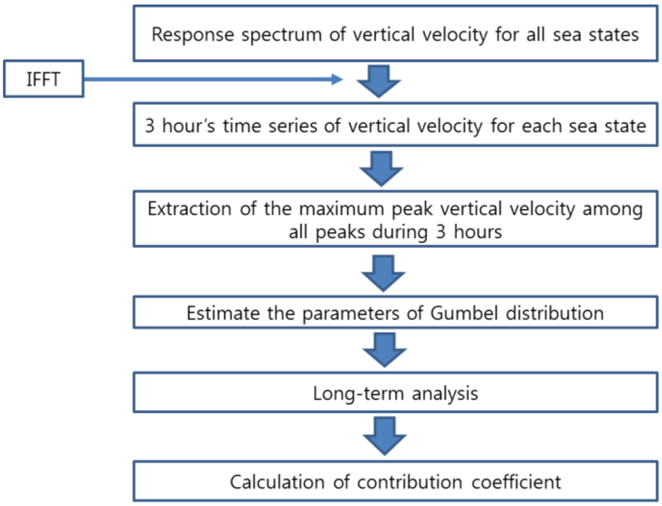

Fig 45 Linear analysis based on Gumbel fit

Fig.46 presents the distribution of contribution coefficient for vertical velocity at ESD for the world−wide scatter diagram. As identified in Fig. 46, the sea states contributing the exceedance probability of long term values is limited.

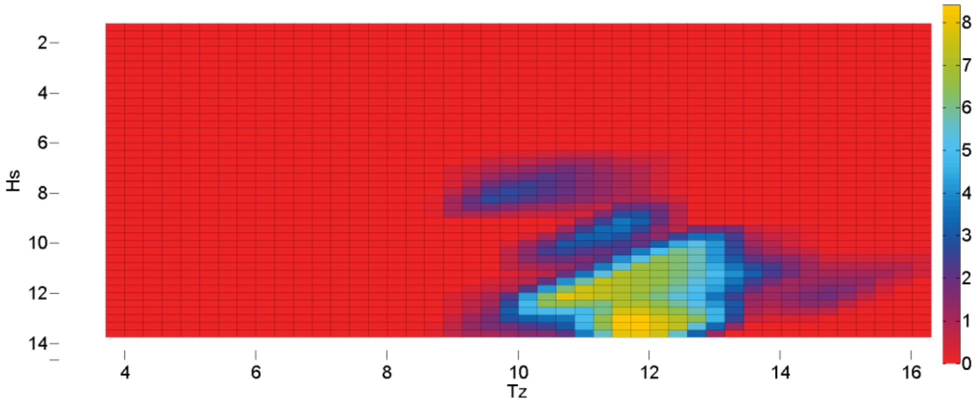

Fig 46 Contribution coefficient for all sea states

The scatter diagram can be divided into two regions. One region contributes to the long−term response to a degree and the other region does not contribute to the long−term response. Total 14 cases of sea states contribute to about 80 % of long−term response in Table 11. Therefore, to reduce computational time, those sea states are used to predict the nonlinear long−term response.

Table 11 Contribution to long−term response

H_S(m)	T_Z(s)	Contribution coefficient (%)
13	9	9
12	8	8
14	8	8
11	7	7
13	7	7

12	7	7
11	6	6
10	6	6
12	5	5
9	4	4
13	3	3
8	3	3
11	3	3
10	3	3
Sum		80

5.2.2. Iteration approach for nonlinear long-term value

Total twenty 3 hours' time series of vertical velocities are generated from its response spectrum obtained from WASIM. For each peak of the time series of vertical velocity, the lifting force and bending moment are calculated using the lifting force contour and the moment contour line. For the resultant 20 maximum peaks for each sea state, the parameters of Gumbel distribution are determined. Then, approximate long term value can be calculated by combining the occurrence probability of the sea state and the Gumbel distribution. This procedure is repeated with adding more sea states around the sea state of the largest contribution until the approximate long−term value converges.

Table 12 shows the change of long−term value by the number of included sea states. Considering head sea only, the long-term value of lift force is converged to 319 (KN) and the moment to 652 (KN-m).

Table 12 Long-term value from iterative approach for lift force

No of sea states	Sea state	long-term value of lift force(KN)
3	H,T(12,10.5),H,T(13,11.5),H,T(14,11.5)	272
6	H,T(11,11.5),H,T(12,10.5),H,T(12,11.5), H,T(13,11.5),H,T(13,12.5),H,T(14,11.5)	292
10	H,T(9,11.5),H,T(10,12.5),H,T(11,12.5), H,T(12,12.5),H,T(11,11.5),H,T(12,10.5), H,T(12,11.5),H,T(13,11.5),H,T(13,12.5), H,T(14,11.5)	305
12	H,T(8,9.5),H,T(13,10.5),H,T(9,11.5), H,T(10,12.5),H,T(11,12.5),H,T(12,12.5), H,T(11,11.5),H,T(12,10.5),H,T(12,11.5), H,T(13,11.5),H,T(13,12.5),H,T(14,11.5)	317
14	H,T(10,10.5),H,T(11,13.5),H,T(8,9.5), H,T(13,10.5),H,T(9,11.5),H,T(10,12.5), H,T(11,12.5),H,T(12,12.5),H,T(11,11.5), H,T(12,10.5),H,T(12,11.5),H,T(13,11.5), H,T(13,12.5),H,T(14,11.5)	319

Table 13 Long-term value from iterative approach for moment

No of sea states	Sea state	long-term value of lift force (KN-m)
3	H,T(12,10.5),H,T(13,11.5),H,T(14,11.5)	567
6	H,T(11,11.5),H,T(12,10.5),H,T(12,11.5), H,T(13,11.5),H,T(13,12.5),H,T(14,11.5)	602

10	H,T(9,11.5),H,T(10,12.5),H,T(11,12.5), H,T(12,12.5),H,T(11,11.5),H,T(12,10.5), H,T(12,11.5),H,T(13,11.5),H,T(13,12.5), H,T(14,11.5)	630
12	H,T(8,9.5),H,T(13,10.5),H,T(9,11.5), H,T(10,12.5),H,T(11,12.5),H,T(12,12.5), H,T(11,11.5),H,T(12,10.5),H,T(12,11.5), H,T(13,11.5),H,T(13,12.5),H,T(14,11.5)	647
14	H,T(10,10.5),H,T(11,13.5),H,T(8,9.5), H,T(13,10.5),H,T(9,11.5),H,T(10,12.5), H,T(11,12.5),H,T(12,12.5),H,T(11,11.5), H,T(12,10.5),H,T(12,11.5),H,T(13,11.5), H,T(13,12.5),H,T(14,11.5)	652

6. Structural analysis

6.1. Description of structural model

The structural analysis is performed using DNV.GENIE as a pre-processor and DNV.SESTRA as a solver. The model is built shown in Fig. 47 and 6 DOF are fixed at the cutting plane of the model in Fig. 48. Steel material of NV-36 in DNV material class is used and the plate thickness distributions are illustrated in Fig. 49 and 50. Plate thickness and detailed structures inside the ESDs are properly assumed due to the absence of relevant drawings. Yield strength of NV-32 is 315N/mm2 and Young's modulus is 2.1x105(MN/m2). Mesh size is 30.0mm x 30.0mm in fine mesh zone and 150.0mm x 150.0 mm as shown in Fig. 51.

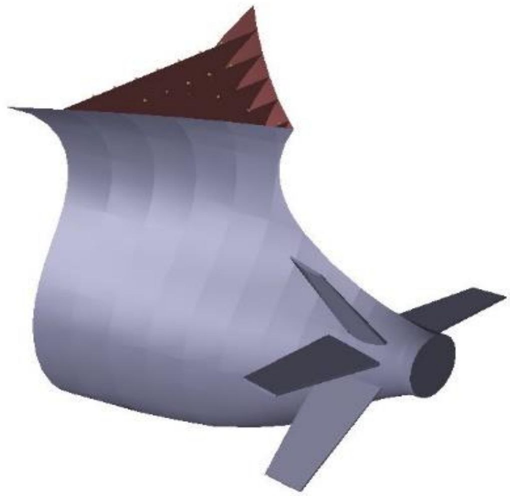

Fig 47 FE model Overview

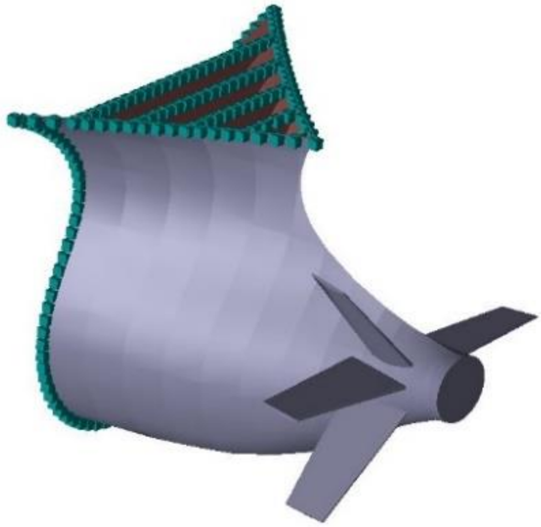

Fig 48 Boundary condition

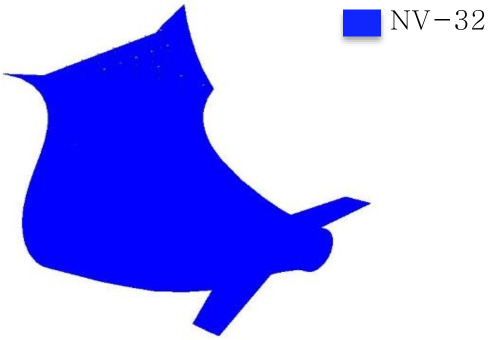

Fig 49 Material

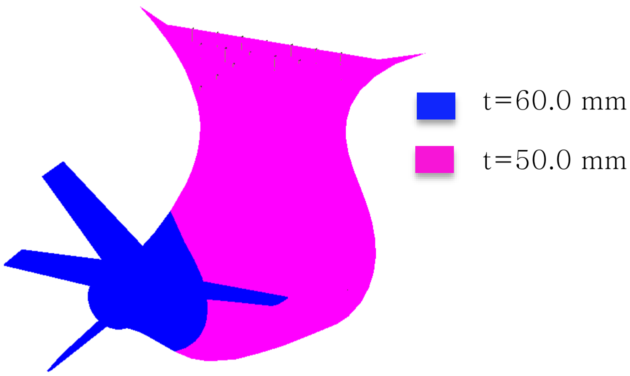

Fig 50 Thickness

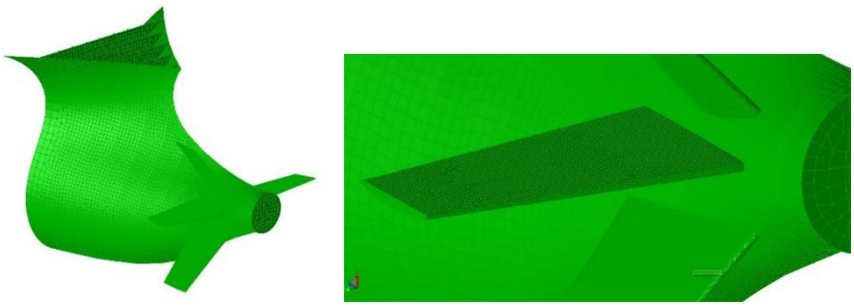

Fig 51 FE mesh

6.2. Application of the hydrodynamic load to structural model

The long–term value of hydrodynamic load is applied to the structural model. Lift force of 258 (KN) and bending moment of 536 (KN–m) considering all heading angles are applied. The loads are realized by applying distributed line load of 258 (KN) at 2.08m distance from the root as shown in Fig. 52. The distance can be calculated by dividing the bending moment value by the lift force, which realizes bending moment at the root as well as the shear force.

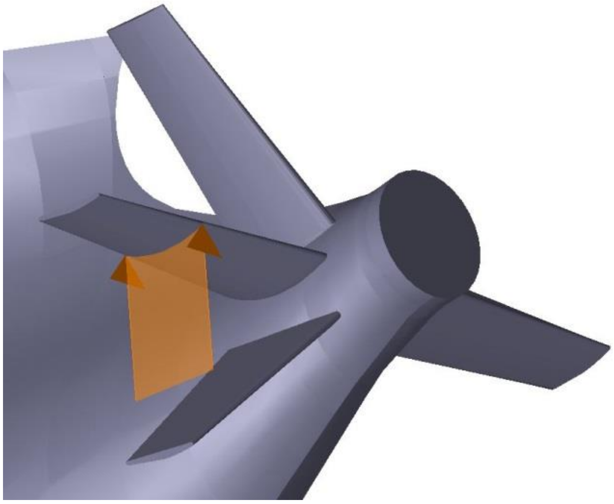

Fig 52 Load application to structural model

6.3. Resultant stress and acceptance criteria

Von-mises distribution from FE analysis results are depicted in Fig. 53 and Fig. 54. The maximum stress occurs at the both ends of hydrofoil root, however, the mesh size of 30x30 mm is sufficiently small and it is limited to local zone.

The structural assessment is to demonstrate that the von Mises stress obtained from the fine mesh finite element analysis do not exceed the maximum permissible stress criteria in accordance with DNV Rules Pt.8 Ch.1 Sec.9 2.3.5.2 [9]. However, this acceptance criteria is based on the assumption of north Atlantic wave environment with design life 25 years while this analysis is based on worldwide wave condition and 20 years design life. Therefore, it is necessary to tune the criteria. In this case, 80% of the original criteria is used for the structural safety assessment because the load ratio in worldwide is generally 80% of that in north Atlantic. Based on the tuned criteria, permissible stress criteria is 362 N/mm2. In this analysis, max von Mises stress is 110 N/mm2.

Table 14 Maximum permissible membrane stresses for fine mesh analysis

Element stress	*Yield utilisation factor*
Element not adjacent to weld	$\lambda_y \leq 1.7$ (load combination S + D) $\lambda_y \leq 1.36$ (load combination S)
Element adjacent to weld	$\lambda_y \leq 1.5$ (load combination S + D) $\lambda_y \leq 1.2$ (load combination S)

Where:

λ_y yield utilisation factor

$= \dfrac{k\ \sigma_{vm}}{235}$ for plate element

$= \dfrac{k\ \sigma_{rod}}{235}$ for rod or beam element

σ_{vm} von Mises stress calculated based on membrane stress at element's centroid, in N/mm^2

σ_{rod} axial stress in rod element, in N/mm^2

k higher strength steel factor, as defined in Section 6/1.1.4 but not to be taken as less than 0.78 for load combination S + D

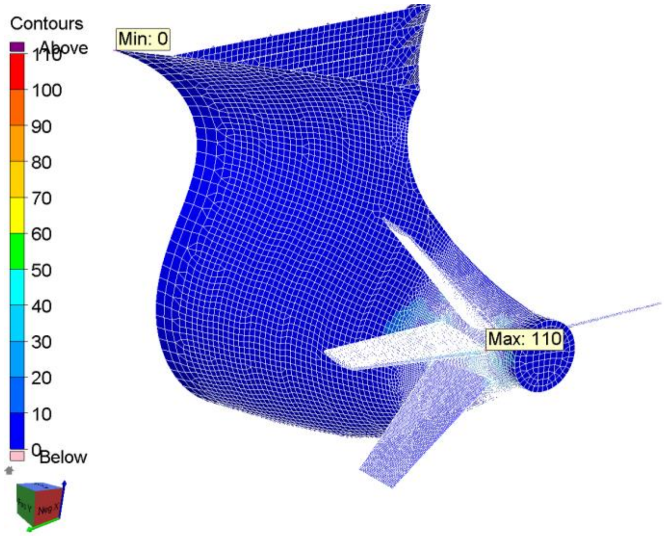

Fig 53 Stress contour – MVONMISES

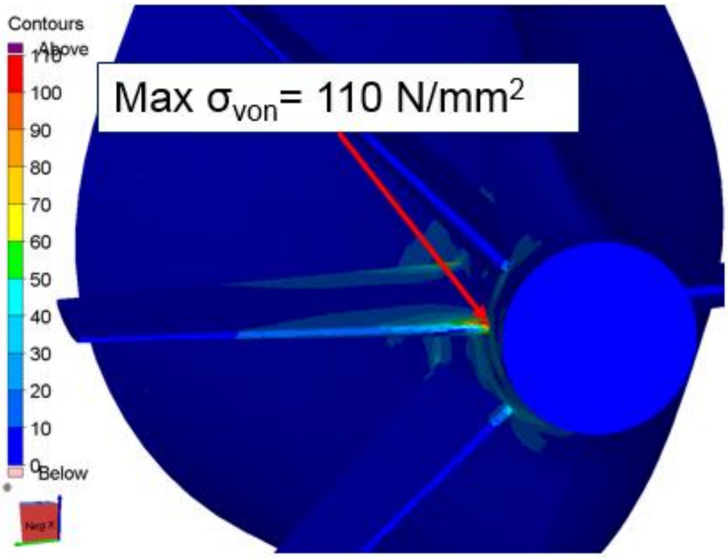

Fig 54 Stress contour – MVONMISES

7. Fatigue strength analysis

7.1. Fatigue strength assessment procedure

A vertical velocity response spectrums at all heading angles are calculated by combining RAO and wave spectrum. Then, irregular time history of vertical velocities is generated form the response spectrum using inverse fourier transform.

Time history of vertical velocity are converted to time histories of lifting force and bending moment using the trained neural network. Then, the time series of lifting force and moment are converted to set of hot spot stress using stress response by unit force. From the results, rainflow counting is performed to reduce a spectrum of varying stress into a set of simple stress reversals. Rainflow counting allows the application of Miner's rule in order to assess the fatigue life of a structure subject to complex loading. Finally, Miner's rule, most widely used cumulative damage model, is used for calculation of fatigue damage. According to DNV CN 30.7, S−N curve I is applied. The detail of procedure of fatigue strength assessment is described in Fig. 55.

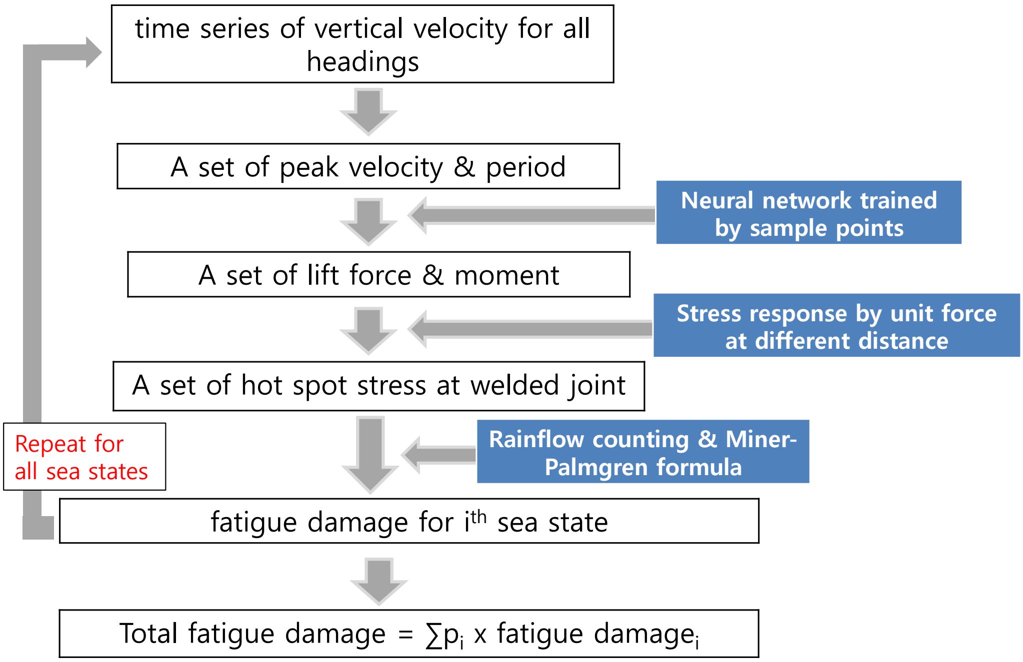

Fig 55 Fatigue strength assessment procedure

According to the above procedure, the calculated fatigue damage and life is 19.41 and 1.03(years), respectively.

7.2. Stress response by unit force

To calculate a set of hot spot stress, it is necessary to convert from lift force and moment to stress response. The ratio between lift force and moment is determined from 0.5 to 11.0 as shown in Fig. 56.

Unit load is applied based on the ratio between lift force and moment and the result of stress response is summarized in Table 15.

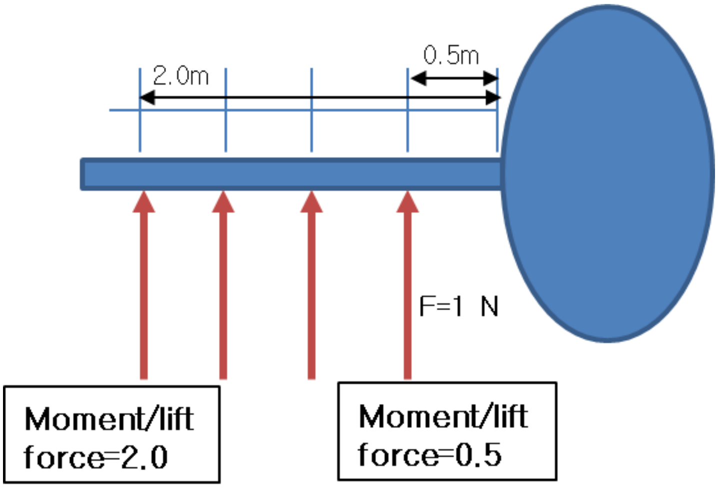

Fig 56 Load application by ratio of lift force and moment

Table 15 Unit stress response

LC	Moment/lift force	Stress (N/mm^2)
1	0.5	−0.0000577
2	1	−0.0001882
3	1.5	−0.0003170
.	.	.
.	.	.
20	10	−0.0023240
21	11	−0.0024416

8. Conclusion

This research performed ship motion analysis using CFD calculation and verified it by comparing with potential-based panel method, DNV.WASIM. From the calculation, hydrodynamic forces imposed on ESDs are calculated.

For an evaluation of long-term value of the hydrodynamic forces, time domain analysis is necessary, however, time-consuming CFD calculation is a main obstacle to the approach. This research proposes a simplified method. Hydrodynamic forces (lift force and bending moment) are calculated for pre-defined regular waves and a neural network is trained for the data. Here, the forces are identified to be affected by wave frequency as well as wave amplitude, therefore, various regular waves with different frequencies and amplitudes are used for the CFD calculation.

Then, irregular time history of vertical velocities is generated form response spectrum obtained from WASIM. In order to take into account the randomness of the irregularity, twenty different irregular time histories are generated.

Then, each time history of vertical velocity is converted to time histories of lift force (shear force) and bending moment. For each sea state, twenty maximum values for 3 hours duration are collected and Gumbel distribution is used to fit the data. This process is repeated for all sea states in wave scatter diagram, and long−term value can be calculated. Approximate long−term calculation is made using contribution coefficient based method, the predicted value are closed to those of Gumbel fitting method.

The calculated values are applied to FE model and its strength assessment is made. The maximum stress occurs at the both ends of hydrofoil root, however, it is limited to local zone. Fatigue analysis is also performed using a stress response by unit force.

Reference

[1] Woo Min, Oh Yeong-Tae, Park Sung-Gun, Jun Seock-Hee, Park Je-Jun and Kim Hee-Chul (DSME), Strength and Fatigue Assessment of Duct Type Energy Saving Device, Proceedings of the Society of Naval Architects of Korea, Jeju, Korea, pp 918-922, May,2013.

[2] O. Boiron, C. Guivier-Curien, E. Bertrand, Study of the hydrodynamic of a flapping foil at moderate angle of attack, Computers & Fluids, Vol.59, pp117-124,2012.

[3] DNV Classification Note No.30.7, Fatigue Assessment of Ship Structures, Det Norske Veritas AS, 2010.

[4] DNV Classification Note No.34.1, CSA-Direct Analysis of Ship Structures, Det Norske Veritas AS, 2013.

[5] DNV Classification Note No.30.5, Environmental conditions and environmental loads, Det Norske Veritas AS, 2000.

[6] Sang Hun Park,Sang Bong Lee,Youn Mo Lee, Study on the Estimation of the Optimum Trims in Container Carriers by using CFD Analysis of Ship Resistances, Journal of the Society of Naval Architects of Korea,Vol.51,pp429-434,2014.

[7] RED Bishop, WG Price. Hydroelasticity of ships. Cambridge University Press: Cambridge, USA, 1979.

[8] Gro Sagli Baarholm, Torgeir Moan, Estimation of nonlinear long-term extremes of hull girder loads in ships, Marine Structures, Vol.13, pp495–516,2000.

[9] DNV Rules Pt.8 Ch.1 Common Structural Rules for Double Hull Oil Tankers with Length 150 meters and above,JULY,2012.

Scatter diagram for world wide trade

HS(m)/Tz(s)	3.5	4.5	5.5	6.5	7.5	8.5	9.5	10.5	11.5	12.5	13.5	14.5	15.5	16.5	17.5	Sum
1	311	2734	6402	7132	5071	2711	1202	470	169	57	19	6	2	1	0	26287
2	20	764	4453	8841	9045	6020	3000	1225	435	140	42	12	3	1	0	34001
3	0	57	902	3474	5549	4973	3004	1377	518	169	50	14	4	1	0	20092
4	0	4	150	1007	2401	2881	2156	1154	485	171	53	15	4	1	0	10482
5	0	0	25	258	859	1338	1230	776	372	146	49	15	4	1	0	5073
6	0	0	4	63	277	540	597	440	240	105	39	13	4	1	0	2323
7	0	0	1	15	84	198	258	219	136	66	27	10	3	1	0	1018
8	0	0	0	4	25	69	103	99	69	37	17	6	2	1	0	432
9	0	0	0	1	7	23	39	42	32	19	9	4	1	1	0	178
10	0	0	0	0	2	7	14	16	14	9	5	2	1	0	0	70
11	0	0	0	0	1	2	5	6	6	4	2	1	1	0	0	28
12	0	0	0	0	0	1	2	2	2	2	1	1	0	0	0	11
13	0	0	0	0	0	0	1	1	1	1	0	0	0	0	0	4
14	0	0	0	0	0	0	0	0	1	0	0	0	0	0	0	1
Sum	331	3559	11937	20795	23321	18763	11611	5827	2480	926	313	99	29	9	0	100000

초록

유체력을 받는 에너지절감장치의 구조적 안전성 평가 절차에 관한 연구

이 동 범

최근 EEDI 의 발효에 따라 환경보호를 위한 CO2절감의 요구와 급증하는 유가로 인한 연료절감에 대한 요구가 맞물려 다양한 타입의 연료절감장치들이 개발되고 있다. 에너지절감장치는 주로 핀이나 덕트 타입으로서 선체후미 및 프로펠러 주변에 유동의 흐름을 따라 부착되어 추진성능을 개선하고 있다. 이와 같은 에너지절감장치에 작용하는 유체력의 크기는 평상시의 운항 때는 그 영향을 무시할 수 있을 정도로 작다. 하지만 악천후에서 운항할 경우 선박의 히브 및 피치운동이 급격히 증가하게 되고 이 경우 핀 타입의 ESD에는 평면 수직방향의 큰 유체력이 작용하게 되어 구조 손상 및 피로파괴의 위험이 커지게 된다. 이러한 에너지절감장치의 구조적 안전성을 평가하기 위하여 기존에는 단순하게 Morison 공식을 사용하여 구조물에 가해지는 유체력을 평가하거나 선형시스템을 가정하여 스펙트랄 방법을 사용하여 유체력을 계산하였다. 하지만 이러한 방법은 유체력의 비선형성을 고려할 수 없기 때문에 정확한 평가가 힘든 단점이 있다.

이러한 이유로 인하여 본 연구에서는 에너지절감장치의 구조적인 안전성을 평가하기 위한 새로운 해석 절차를 제안하고 제안된 절차를 기존의 핀 타입의 에너지절감장치에 적용하였다.

새롭게 제안된 구조안전성평가 절차에서는 ULS 와 FLS를 검증하였으며 그 과정은 크게 seakeeping analysis, CFD analysis 및 long-term analysis로서 3가지 단계로 나뉜다.

첫 번째 단계인 seakeeping analysis단계에서는 상용운동해석 코드인 WASIM을 이용하여 선박의 ESD위치에서의 수직방향속도의 RAO 및 응답스펙트럼을 계산하게 된다. 그리고 생성된 수직방향의 응답스펙트럼을 Inverse Fast Fourier transform을 통하여 3시간동안의 수직방향속도의 시계열 자료로 변환하게 된다. CFD analysis 단계에서는 앞에서 계산된 수직방향속도의 최대값들을 neural network를 사용하여 각각 양력 및 모멘트로 변환시켜준다. 이를 위해 운동해석으로부터 미리 선정된 파고 및 주기에 대해 CFD 해석을 실시하여 ESD에 작용하는 양력 및 모멘트를 계산하게 되고 이 결과를 이용하여 neural network를 학습시킨다. 임의성을 반영하기 위하여 하나의 해상상태 당 20개씩의 수직방향속도 시계열자료를 생성하게 되고 neural network를 통해 변환된 양력과 모멘트 결과를 이용하여 Gumbel 분포의 parameter를 선정한다. 이와 같은 과정을 wave scatter diagram에 있는 모든 해상상태에 대해 반복하고 long-term analysis를 통해 최종적으로

long-term값을 계산하게 된다.

앞에서 설명한 long-term analysis에 추가적으로 기여계수를 이용한 approximate long-term analysis를 이용하여 long-term 값을 구하고 그 결과를 앞에서 구한 결과와 비교해보았다. 기존의 long-term analysis는 모든 해역에 대해 해석을 수행하기 때문에 방대한 시간이 소요되는 단점이 있지만 기여계수를 이용한 approximate long-term analysis의 경우에는 미리 선형해석을 통해 long-term value에 가장 크게 기여하는 해상상태를 찾고 그 해상상태부터 비선형해석을 실시하여 최종적으로 수렴하는 long-term값을 찾는 방법이기 때문에 해석에 수행되는 시간을 크게 줄일 수 있다는 장점이 있다.

극한강도를 평가하기 위한 과정 다음으로 피로강도를 평가하기 위한 절차를 수립하였다. 수직방향속도의 응답스펙트럼으로부터 3시간동안의 시계열 자료를 생성하고 이 때의 모든 최대값들을 앞에서 훈련된 neural network를 사용하여 양력 및 모멘트로 변환시켰다. 그리고 생성된 양력과 모멘트의 시계열 자료를 다시 미리 단위하중에 의해 계산된 stress의 응답을 이용하여 stress histogram으로 변환하였고 최종적으로 miner's rule을 사용하여 피로수명을 계산하였다.

주요어: ESD(Energy Saveing Device), CFD(Computational Fluid Dynamics), Neural network, Long-term analysis

학 번: 2013-21074